ACS Biomaterials SCIENCE & ENGINEERING

Controlled Release and Delivery Systems

Intratumorally Injected Photothermal Agent-Loaded Photodynamic Nanocarriers for Ablation of Orthotopic Melanoma and Breast Cancer

Xiaodong Sun, Bo Zhuang, Mengmeng Zhang, Heliu Jiang, and Yiguang Jin

ACS Biomater. Sci. Eng., **Just Accepted Manuscript** • DOI: 10.1021/acsbiomaterials.8b01111 • Publication Date (Web): 01 Jan 2019

ACS Publications

is published by the American Chemical Society. 1155 Sixteenth Street N.W., Washington, DC 20036

Intratumorally Injected Photothermal Agent-Loaded Photodynamic Nanocarriers for Ablation of Orthotopic Melanoma and Breast Cancer

Xiaodong Sun,[†,‡] Bo Zhuang,[†] Mengmeng Zhang,[†,‡] Heliu Jiang,[†] and Yiguang Jin[*,†,‡]

[†]Department of Pharmaceutical Sciences, Beijing Institute of Radiation Medicine, 27 Taiping Road, Beijing 100850, China, e-mail address: jinyg@sina.com

[‡]Institute of Pharmacy, Pharmaceutical College of Henan University, Jin Ming Avenue, Kaifeng 475004, China

ABSTRACT: Traditional chemotherapy of cancers may lead to serious adverse reactions due to little drug distribution in tumors. Here, a combination of photothermal therapy (PTT) and photodynamic therapy (PDT) was used for local treatment of orthotopic melanoma and breast cancer via intratumoral (i.t.) injection of photothermal agent-loaded photodynamic nanocarriers. A hydrophobic derivative of indocyanine green, DCC, was synthesized and entrapped into a pH-sensitive photosensitizer-core copolymer, PDCZP, to form DCC@PDCZP. The nanocarriers showed remarkable fluorescence, high singlet oxygen quantum yields, and strong photothermal effect. Flow cytometry suggested that the nanocarriers were efficiently internalized by cancer cells. Near infrared thermal imaging and fluorescence self-imaging showed that the i.t. injected DCC@PDCZP mainly remained in the tumors but the intravenous (i.v.) nanocarriers were distributed a little. One i.t. injection of DCC@PDCZP was enough to ablate the orthotopic B16-F10 and 4T1 mouse tumors under 830 nm and 660 nm irradiation at 4 hours post-injection. More importantly, no local recurrences were found though swabs were formed at 9 days post-treatment. The major anticancer mechanisms included improvement of cancer cell necrosis due to hyperthermia, inhibition of neovascularization, and enhancement of cell apoptosis. The i.t. injection of PTT/PDT nanoformulations is thus a promising local treatment of superficial tumors.

KEYWORDS: *breast cancer; indocyanine green; intratumoral injection; melanoma; photodynamic therapy; photothermal therapy; zinc phthalocyanine*

INTRODUCTION

Nanocarriers are widely used as tumor-targeted delivery systems, and intravenous (i.v.) injection of them is a preferred option because the enhanced permeability and retention (EPR) effect is regarded as the basis of *in vivo* tumor targeting of nanoscale systems.[1] However, the EPR effect is now seriously doubted because it has hardly been validated in human bodies.[2-3] Moreover, several marketed anticancer nanoscale formulations (e.g., Doxil®, Abraxane®) show little higher survival percentages than their free drug solutions.[4] If nanoscale systems have no significant tumor targeting effect, what's the prospect of nanocarriers?

Cutaneous melanoma is a severe skin cancer with high incidence rates in western countries and an estimated 76,380 new cases occurred in the United States in 2016,[5] which is the leading cause of death in superficial tumors.[6-7] Traditional treatments of melanoma include surgical resection, chemotherapy, and radiotherapy.[8] Another common type of superficial tumors is breast cancer that is the leading malignant tumor in women with 1.7 million new cases worldwide in 2012. While significant progress has been made in breast cancer diagnosis and early treatment, this malignancy still accounts for over half a million deaths yearly.[9] Recurrence of breast cancer in the front chest wall after mastectomy and radiotherapy poses a major problem, as limited therapeutic options remain for clinical application.[10] Oral administration and i.v. injection are the major approaches to chemotherapy. However, the amount of a drug that makes its way into the tissues of melanoma or breast cancer is very limited due to wide drug distribution in the body. Moreover, currently clinically applied anti-melanoma or breast cancer drugs have no sufficient capacity to differentiate cancer cells from normal cells, which leads to serious adverse reactions among patients.[11] Therefore, an effective treatment with weak or without side effects is emergent for therapy of melanoma and breast cancer. Moreover, the monotherapy of cancer generally does not produce satisfactory results so that a combination therapy assumes new importance due to various action mechanisms of different treatments to enhance anticancer efficiency and reduce side effect.[12]

Recently, photodynamic therapy (PDT) and photothermal therapy (PTT) have been studied a lot due to their noninvasive property, no drug resistance, significant therapeutic efficacy, low side effect, and manually control by light irradiation.[13-15] PDT is a local treatment of diseases based on light, photosensitizers and oxygen. Highly efficient PDT of cancer includes two key steps: photosensitizers enter cancer cells and then are excited by an appropriate light. Reactive oxygen species (ROS) and singlet oxygen (^1O) are produced and cancer cells are killed via apoptosis or necrosis.[16-17] Because singlet oxygen has a short half-life of 40 ns and a short diffusion distance of 10−20 nm, cell uptake of the photosensitizers is critical to PDT.[18-19] Hyperthermia is an alternative way for efficient therapy for cancer and has already been documented.[20] As another phototherapeutic method, PTT is based on photothermal agents which strongly absorb near infrared (NIR) light and convert it into heat to destroy surrounding cancer cells, such as indocyanine green (ICG), gold nanoparticles, or carbon nanotubes. PTT has been demonstrated as a noninvasive, harmless and highly efficient therapeutic technique.[21-22] In order to achieve the best effect of PTT, photothermal agents of an appropriate dose need to reach the tumor tissues after systemic or local administration. High tumor targeting or distribution of drugs is difficult to achieve by systemic administration, though a lot of nanocarriers has been applied. Actually, only less than 1% of drugs may be delivered to tumor tissues via nanocarriers.[23] Against this context, intratumoral (i.t.) injection which might increase the concentration of drugs in tumor tissues and reduce systemic toxicity could be a better means of administration for PDT and PTT.[24-25]

Here, a hydrophobic derivative of ICG was prepared as a photothermal agent, which was entrapped into a pH-responsive zinc phthalocyanine copolymer nanocarrier. Hydrophobic photosensitizers may be well entrapped in this copolymer. However, the *in vivo* toxicity of most of them has not been enough explored, such as quantum dots,[26] polyaniline,[27] polypyrrole,[28] and so on. ICG is a not only water-soluble clinically applied fluorescent contrast agent and but also acts as a photothermal agent. Its *in vivo* safety has been ensured and approved by the FDA.[29] However, ICG is not stable in solutions and is rapidly eliminated from the blood circulation with only 2−4 min of $t_{1/2}$, leading to limited clinical application.[30] We synthesized the derivative of ICG, i.e., DCC, after introducing a chloride atom, a rigid circle and an ethyloxycarbonylethyl group to the ICG fluorophore, to achieve cellular toxicity, high stability, and hydrophobicity. Hydrophobicity makes it easy for DCC to get entrapped in the cores of nanoparticles or polymeric micelles. PDCZP is a pH-sensitive copolymer synthesized in our lab.[31] It can release the entrapped drugs in the environment at low pH due to the hydrophobic-hydrophilic transition of the pDEA group. Moreover, PDCZP would likely release entrapped drugs in the low pH environment of tumor tissues and from the lysosomes after internalization by cancer cells. Therefore, the combination of DCC and PDCZP would likely take high entrapment of photothermal agents, high stability, and rapid release in the tumors. The drug-loaded nanocarriers were injected into the tissues of orthotopic mouse melanoma and breast cancer. The i.t. injection of the nanocarriers resulted in ablation of melanoma and breast cancer and no local recurrences were observed compared to the control at 9 days post-injection. The highly efficient therapy was explored and the mechanisms were analyzed.

EXPERIMENTAL SECTION

Materials. The pH-responsive photosensitizer-core four-armed star-shaped copolymer, i.e., [methoxy-poly(ethylene glycol)-poly(2-(N,N-diethylamino)ethyl methacrylate)-poly(ε-caprolactone)]$_4$-zinc β-tetra-(4-carboxyl benzyloxyl)phthalocyanine (PDCZP) was synthesized in our previous research,[31] except for the replacement of methoxy-poly(ethylene glycol) 2000 with methoxy-poly(ethylene glycol) 750. A copolymer with a short PEG chain, i.e., (mPEG$_{750}$-pDEA-pCL)$_4$-ZnPC$_4$, PDCZP in this study, was finally obtained. Mitoxantrone chloride was purchased from Beijing Yikang Co., Ltd., China. Other reagents, including 2,3,3-trimethylbenzoindolenine, ethyl 4-bromobutyrate (EBB) and ICG, were purchased from Beijing Ouhe Technology Co., Ltd. 9,10-Dimethylanthracene (DMA) and zinc phthalocyanine (ZnPc) were from TCI

(Tokyo, Japan). Organic solvents were of analytical grade and other chemicals were of reagent grade. Fetal bovine serum, RMPI 1640, DMEM and trypsin-EDTA were purchased from Gibco Life Technologies (USA). DAPI and Lyso-tracker red markers were purchased from Beyotime Biotechnology (Shanghai, China). Purified water was prepared using the Heal Force Super NW Water System (Shanghai Canrex Analytic Instrument Co., Ltd., Shanghai, China). Dialysis bags were purchased from Union Carbide Corporation (New Jersey, USA).

Synthesis of the Photothermal Agent DCC. The photothermal agent, diethyl chloro-cylcohexenyl cypate, i.e., DCC, was synthesized as follows (Figure S1 in the supporting information). Two intermediates, **1** and **2**, were prepared according to the literature with slight modifications.[32] A solution of $POCl_3$ (9.5 mL, 42.9 mmol) in dichloromethane (DCM, 19.5 mL) was slowly added to an ice-cooled solution of N,N-dimethyl foramide (DMF, 10 mL, 103.2 mmol) in DCM (10 mL). Then, cyclohexanone (2.5 g, 6.25 mmol) was added to the reaction solution and refluxed for 3 hours at 50 °C. The mixture was cooled with ice. Ice pieces (50 g) were slowly added in the stirred mixture followed by agitation for 30 min. The DCM phase was collected and the water phase was extracted with additional DCM. The DCM solutions were combined and passed through an $MgSO_4$ column. The solvent was removed from the solution under vacuum. The crude product was purified with a silica gel column and an eluting solvent of DCM:MeOH (30:1, v/v), to obtain 2-chloro-1-formyl-3-(hydroxymethylene)cyclohex-1-ene (**1**) as a yellow crystalline solid. Nuclear magnetic resonance (NMR) spectra and mass spectra were recorded using a JNM-ECA-400 NMR spectrometer and a Perkin-Elmer Sciex API-3000 MS spectrometer, respectively. ^{1}H NMR ($CDCl_3$, 400 MHz) δ ppm: 1.66−1.74 (m, 2H, CH_2), 1.77−2.11 (m, 4H, $2CH_2$), 2.71 (s, 1H, CH), 2.92 (d, 2H, CH_2, J = 4.2 Hz), 3.02 (s, 1H, OH), 10.02 (s, 1H, CH=O); ESI-MS (+), m/z: 173 (M^+).

2,3,3-Trimethylbenzoindolenine (0.74 g, 3.5 mmol) and EBB (3.7 g, 18.7 mmol) were together refluxed at 120 °C for 2 hours, and diethyl ether (300 mL) was added to the system. The mixture was stirred at room temperature for 13 hours. The precipitate was recrystallized from DCM and ethyl acetate. The crude product was purified through a silica gel column by eluting with DCM:MeOH (30:1, v/v). 1-Ethyloxycarbonylethyl-2,3,3-trimethylbenzoindoleninium bromide (**2**) was obtained as a purple solid. ^{1}H NMR ($CDCl_3$, 400 MHz) δ ppm: 1.24 (s, 6H, $2CH_3$), 1.87 (s, 3H, CH_3), 2.05 (s, 2H, CH_2), 2.70 (s, 2H, CH_2), 3.27 (s, 3H, CH_3), 3.49 (s, 2H, CH_2), 4.14 (t, 2H, CH_2, J = 3.36Hz), 7.65−7.76 (m, 2H, ArH), 7.93−8.12 (m, 2H, ArH), ESI-MS (+), m/z: 324.20 (M^+).

Compounds **1** (78.5 mg, 0.5 mmol), **2** (354 mg, 1.0 mmol) and sodium acetate (41.0 mg, 0.5 mmol) were dissolved in acetic anhydride (10 mL) and stirred at room temperature for 2 days. The dark green solution was poured into ethyl ether (200 mL) and filtered. The collected precipitate was purified by the silica gel chromatography (DCM:MeOH, 99:1−95:5, v/v) to obtain DCC as a dark green solid. The synthetic procedure and NMR spectrum of DCC are in the supporting information.

UV-Vis Absorption and Fluorescence of DCC and PDCZP. DCC solutions in methanol and PDCZP solutions in tetrahydrofuran (THF) were scanned in the range of 200−900 nm on a TU-1901 spectrophotometer (Beijing Purkinje General Instrument Co., Ltd., Beijing, China). A DCC solution in dimethyl sulphoxide (DMSO) was prepared with the absorbance of ~0.7 at the maximal wavelength of 835 nm, and then 100-fold diluted with DMSO. The dilution was scanned using a fluorescent spectrophotometer (Cary Eclipse, VARIAN, USA) to find the maximal excitation and emission wavelengths, i.e., λ_{ex}, λ_{em}.

Quantification of DCC, PDCZP and Mitoxantrone. A DCC-contained sample was dissolved in methanol and DCC was determined using a spectrophotometry at 830 nm. PDCZP was a conjugate of three polymer blocks and a photosensitizer core, i.e., PEG, PDEA and PCL and $ZnPC_4$. These polymer blocks had no absorption though $ZnPC_4$ had a maximal absorption wavelength of 673 nm. Therefore, PDCZP was determined using a spectrophotometry at 673 nm after the sample was dissolved in THF in the dark. Mitoxantrone was determined using the high-performance liquid chromatography (HPLC) with reference to the China Pharmacopeia as follows: an Agilent 1260 HPLC instrument, a Dikma Diamonsil C18(2) HPLC column (5 μm, 250 mm × 4.6 mm) at 30 °C, a mobile phase of acetonitrile/sodium 1-hepatanesulphonate solutions (30:70, v/v) at the flow rate of 1 mL/min, the injected volume of 20 μL, and the detection wavelength of 244 nm. A sodium 1-hepatanesulphonate solution was prepared by dissolving 2.2 g of sodium 1-hepatanesulphonate into water, adding 3.2 mL of acetic acid, and diluting the mixture to 365 mL with water. The retention time of mitoxantrone was about 24 min.

Measurement of DCC Photostability. A DCC solution in methanol was prepared with an absorbance in the range of 0.8−1.0. The photostability of DCC was measured at 830 nm after continual 250 mW/830 nm light irradiation on the DCC solution with an interval of 2 min up to 32 min. An 830 nm diode laser emitter (Lasever Inc., Ningbo, China) was used. Light intensities were measured using Nova II (OPHIR, Israel).

Fluorescence Quantum Yield Measurement of DCC and PDCZP. The area under the fluorescence emission spectra of DCC and ICG solutions in DMSO was integrated as S_{DCC} and S_{ICG}, respectively. Their absorbance at 835 nm was also measured, as A_{DCC} and A_{ICG}, respectively. The fluorescence quantum yield ($\Phi_{F/ICG}$) of ICG in DMSO was 0.12.[33] Therefore, the $\Phi_{F/DCC}$ was calculated as Eq. (1).[34]

$$\Phi_{F/DCC} = 0.12\frac{S_{DCC}A_{ICG}}{A_{DCC}S_{ICG}} \qquad (1)$$

A PDCZP solution in DMF was prepared with the absorbance of about 0.7 at 673 nm. It was 100-fold diluted with DMF and the fluorescence quantum yield ($\Phi_{F/PDCZP}$) of PDCZP was measured as Eq. (2) with the $\Phi_{F/ZnPc}$ of 0.30.[34]

$$\Phi_{F/PDCZP} = 0.30\frac{S_{PDCZP}A_{ZnPc}}{A_{PDCZP}S_{ZnPc}} \qquad (2)$$

Singlet Oxygen Quantum Yield Measurement of PDCZP. The singlet oxygen quantum yield (Φ) of PDCZP in DMF was measured with the same method in our previous research.[31] The test was based on the changes of a singlet oxygen chemical quencher, 9,10-dimethylanthracene (DMA, TCI, Tokyo, Japan) in DMF. A 100 mW/660 nm laser emitter (YSHINELASER, China) was used. Briefly, light irradiation was conducted on a series of solutions containing ZnPc, PDCZP, and/or DMA. Singlet oxygen quantum yields (Φ) of photosensitizers were calculated according to DMA oxidation rates. Φ_{PDCZP} was calculated after comparison with the known Φ_{ZnPc} (0.56) of ZnPc in DMF.

Preparation of DCC@PDCZP. DCC and PDCZP of 1:2 (w/w) were dissolved in THF and water was injected into the solution under bath ultrasound with a 100-μL syringe. The organic solvent in the suspension was removed at 37 °C under vacuum to obtain a DCC@PDCZP suspension containing 250 μg DCC/mL. A PDCZP suspension and a fluorescein isothiocyanate (FITC)@PDCZP (1:5, w/w) suspension were also prepared as above.

Photothermal Effect of DCC and DCC@PDCZP. A 250 μg/mL DCC solution in DMSO was prepared and diluted with water to 1, 2, 5, 10, 25, 50 and 100 μg/mL. The diluted solutions remained stable within 5 hours without obvious agglomerates. An aliquot (0.5 mL) of the above solutions was put into a 1.5-mL plastic centrifuge tube. Vertical laser irradiation was performed on the tube with 830 nm and 1 W/cm^2. The sample temperature was measured with the temperature meter attached to a pH meter (HI2221, HANNA, GE) at 0, 30, 60, 120, 150, 180, 210, 240, 270 and 300 s. A DCC@PDCZP suspension in water was prepared, containing 250 μg DCC/mL. It was diluted with water to the same concentrations as the above DCC dilutions. The photothermal effect of DCC@PDCZP was also measured as above.

Transmission Electron Microscopy, Size and Zeta Potential of PDCZP and DCC@PDCZP. PDCZP and DCC@PDCZP were observed under a Hitachi H-7650

80 kV transmission electron microscope (TEM) after staining with sodium phosphotungstate solutions (pH 7.4). A dynamic light scattering (DLS) method on Zetasizer Nano ZS (Malvern, UK) was used for measuring the sizes of PDCZP and DCC@PDCZP at different pH. The zeta potential of PDCZP and DCC@PDCZP was also measured using the above instrument at 25 °C.

Encapsulation and Loading Efficiencies of DCC in DCC@PDCZP. DCC@PDCZP suspensions were centrifuged through ultrafiltration tubes (cutoff MW, 10,000, PALL Corporation, USA) at 5,000× g for 10 min. Free DCC in the filtrate was determined on the UV-vis spectrophotometer at 830 nm. The encapsulation efficiency (EE) and loading efficiency (LE) of DCC were calculated as Eq. (3) and (4).

$$EE = (\text{Encapsulated DCC})/(\text{Totally added DCC}) \times 100\% \qquad (3)$$

$$LE = (\text{Encapsulated DCC})/(\text{Total amount of DCC@PDCZP}) \times 100\% \qquad (4)$$

Release of DCC from DCC@PDCZP. An aliquot (1 mL) of DCC@PDCZP suspensions (250 μg DCC/mL) was put into a dialysis bag (cutoff MW, 3,500) that was then immersed in 10 mL of 37 °C phosphate buffered solutions (PBS, pH 7.4, 6.5, or 5.0) containing 8% Tween 80. The dissolution system was incubated at 37 °C under vibration at 150 rpm. At the predetermined time points, 1 mL of the media was withdrawn for the spectrophotometric assay of released DCC at 830 nm after dilution with methanol (1 mL) and ultrasound for 5 min. An equal volume of media was supplemented into the media at the same time.

Hemolysis Assay of DCC and PDCZP. Rat erythrocyte suspensions (2%, v/v) in saline were prepared according to the report.[35] A series of samples were prepared, containing 1% erythrocytes and a series of PDCZP or DCC suspensions including 5, 4, 3, 2 and 1 mg/mL in saline and they were incubated at 37 °C until observation. Hemolysis was observed with naked eyes against the completely hemolytic sample of water-mixed erythrocytes. Three hours later, the supernatants were also collected and the absorbance at 577 nm was measured.

Phototoxicity of light irradiation at 830 nm and 660 nm. B16-F10 mouse melanoma cells and 4T1 mouse breast cancer cells were used. Cells were grown in the DMEM (for B16-F10 cells) or RMPI 1640 (for 4T1 cells) culture media containing 10% fetal bovine serum at 37 °C under 5% CO_2. The B16-F10 or 4T1 cells were seeded into 96-well plates (5×10^3 cells/well). Phototoxicity on cells was assayed by directly light irradiation at 830 nm (1 W/cm^2) or 660 nm (200 mW/cm^2) for 30, 60, 90, 120, 240 and 300 s. The cells were incubated at 37 °C for 24 hours. The cell viability of B16-F10 and 4T1 cells was measured using the MTT method. An aliquot (20 μL) of MTT solutions was added to each well. The plates were maintained at 37 °C for 4 hours. The culture media were discarded, and DMSO (150 μL) was added to dissolve dark-blue formazan crystals. Formazan was measured at 490 nm using a microplate reader (Mul-tiskan MK3, Thermo Scientific, US). Cell viability was equal to (absorbance of sample)/(absorbance of control) × 100%.

Dark Cytotoxicity of DCC, PDCZP and Mitoxantrone. The dark toxicity of regimens was evaluated on B16-F10 cells that were seeded into 96-well plates (5×10^3

cells/well) and cultured overnight. Cells were incubated with a series of PDCZP (25−200 μg/mL), DCC (0.5−200 μg/mL), and mitoxantrone (0.5−200 μg/mL) solutions for 24 hours under darkness, respectively. Cell viability was measured using the MTT method.

Cell incubation Time Under Darkness. The incubation time under darkness before photodynamic treatment was investigated. B16-F10 or 4T1 cells were seeded into 96-well plates ($5×10^3$ cells/well) and incubated for 24 hours. The media were replaced with a series of DCC or DCC@PDCZP suspensions containing 5−200 μg DCC/mL, and incubated for 1, 2, 3 and 4 hours, respectively. The cell viability was measured using the MTT method.

In Vitro Photodynamic and Photothermal Studies of DCC and DCC@PDCZP. A series of DCC or DCC@PDCZP suspensions were prepared with 20−200 μg DCC/mL and a series of PDCZP suspensions were prepared with 20−200 μg PDCZP/mL. B16-F10 or 4T1 cells were seeded into 96-well plates ($5×10^3$ cells/well) and incubated for 24 hours. The media were replaced with/without the above DCC, PDCZP and DCC@PDCZP suspensions, respectively. Two hours later, the wells were light-irradiated or not in the following groups: non-irradiation, DCC, DCC with 830 nm irradiation, PDCZP, PDCZP with 660 nm irradiation, 830 nm and then 660 nm irradiation, DCC@PDCZP, DCC@PDCZP with 830 nm and 660 nm irradiation, and blank control. The irradiation conditions included: (1) 830 nm and 1.0 W/cm^2 irradiation for 3 min; (2) 660 nm and 200 mW/cm^2 irradiation for 3 min; (3) continual irradiation using (1) and (2) by turns. After irradiation, the cells were incubated for 1 hour under darkness. Cell viability was measured using the MTT method.

In Vitro Cellular Uptake of DCC and DCC@PDCZP and Its Localization in cells. B16-F10 mouse melanoma cells (1×10^5 cells/well) were seeded in 6-well plates and incubated at 37 ºC for 1 h. An aliquot (100 μL) of FITC@PDCZP was added to the wells. After incubation for 1, 2, 4, 8 and 12 hours, the cells were washed 3 times with PBS, processed with trypsin, centrifuged at 4 °C, and finally re-suspended in 0.5 mL of PBS. The fluorescent intensities of FITC in cells were analyzed using a flow cytometry (BD FACS Calibur, USA). In addition, the cellular uptake of DCC@PDCZP and free DCC in DMSO (both of them containing 10 μg DCC/mL) was also investigated after incubation with the cells for 4 hours. The cells were washed with PBS and homogenated using an ultrasonic homogenizer (80W, HUP-100, Tianjin Hengao Technology Development Co., Ltd., China) with the power at the 2nd grade for 20 s (1s each time with 1 s interval). The homogenates were thoroughly mixed with methanol (3 mL/well) and centrifuged at 5,000 rpm for 5 min. DCC in the supernatants was determined using a spectrophotometry at 830 nm. The cell-internalized DCC was calculated.

The 4T1 cells (2×10^5 cells/well) were seeded in 35-mm dishes with coverslips at the bottoms and incubated at 37 °C in 5% CO_2 for 24 hours. The culture media were replaced with the DCC@PDCZP suspensions containing 40 μg PDCZP/mL and the cells were incubated for another 4 hours. The cells were irradiated using the light of 830 nm and 1.0 W/cm^2 for 3 min or not. The cells on the coverslips were washed three times with PBS, stained by the Lyso-tracker red marker for 30 min, fixed by 4% paraformaldehyde for 15 min, and then stained using DAPI for 5 min. The cells were washed thoroughly with PBS and mounted on glass slides. The images of cells were taken using a Nikon TiE-A1 confocal laser scanning microscope (CLSM).

Animal Models of Orthotopic Melanoma and Breast Cancer. Female BALB/c nude mice (18−20 g) were purchased from the SPF (Beijing) Biotechnology Co. Ltd, China. The handling and surgical procedures of animals were conducted in strict accordance with the Guide for the Use of Laboratory Animals of Beijing Institute of Radiation Medicine. B16-F10 cells (0.1 mL, 1×10^7 cells) or 4T1 cells (0.1 mL, 1×10^7 cells) were inoculated into the mice under the right forelimb by subcutaneous (s.c.) injection. Seven days post-inoculation, the mice with an appropriate tumor volume (ca. 200 mm^3) were selected for the studies of tissue distribution and pharmacodynamics. Tumor volume (V) was calculated as $V = a \times b^2/2$, where a was the length of tumor, and b was the width of tumor.

Tumor Temperature Measurement under Light Irradiation. B16-F10 or 4T1 tumor-bearing nude mice were each i.t. injected with 100 μL of DCC@PDCZP (containing 50 μg DCC/mL). Tumor-bearing mice without treatment were used as the control. The tumors were irradiated under 830 nm and 1.0 W/cm^2 laser for 3 min. Regional infrared thermographic maps were obtained using an infrared thermal imaging camera (THERMOVISION A40, FLIR, USA) and the temperature was deduced.[36]

In Vivo Imaging of DCC@PDCZP. B16-F10 or 4T1 tumor-bearing nude mice were randomly divided into two groups (two mice per group), wherein two mice were i.v. injected with 100 μL of DCC@PDCZP (containing 50 μg DCC/mL) and the others were i.t. injected. Fluorescence imaging of the B16-F10 tumor-bearing mice was conducted at 0.5, 1, 2, 4, 6, 8 and 12 hours post-injection using an *in vivo* imaging system (IVIS Lumina, USA) at an excitation wavelength of 745 nm and an 820 nm filter to collect the fluorescence (FL) signals of DCC. The 4T1 tumor-bearing mice were also treated as above up to 24 h.

In Vivo Photothermal and Photodynamic Therapy of PDCZP, DCC, and DCC@PDCZP. Thirty-six B16-F10 tumor-bearing mice were equally divided to nine groups. The mice in Group a served as controls that were only i.t. injected with PBS. The mice in Groups b, c, d and e were i.t. injected with PDCZP, DCC, DCC@PDCZP and mitoxantrone, respectively. The mice in Groups a–e were not irradiated. The mice in Groups f–i were light-irradiated while the mice in Group f were i.t. injected with PDCZP and then irradiated with 660 nm laser. The mice in Group g were i.t. injected with DCC and then irradiated with 830 nm laser. The mice in Group h were injected with DCC@PDCZP, and then irradiated with 830 nm and sequential 660 nm laser one hour later. The mice in Group i were irradiated with 830 nm and then 660 nm laser as the same as Group h but without any administered regimens. All the laser zones completely covered the tumor xenografts. For Groups a–e, an aliquot (100 μL) of various regimens, including saline, PDCZP (680 μg/mL), free DCC (100 μg/mL aqueous suspensions), DCC@PDCZP (containing 100 μg/mL DCC and 680 μg/mL

PDCZP), and mitoxantrone (200 μg/mL) was i.t. injected on Days 1, 3, 5 and 7. For Groups f–h, the i.t. injection and light irradiation at 4 hours post-injection were performed only once, where the mice in Group f underwent the 660 nm and 200 mW/cm^2 irradiation for 5 min only, those in Group g underwent the 830 nm and 1.0 W/cm^2 irradiation for 3 min, and those in Group h underwent the above 830 nm and 660 nm irradiation in turn. The mice in Group i underwent the above 830 nm and 660 nm irradiation only once without injection of any regimens. The mice were finally sacrificed 9 days post-injection. A pharmacodynamic study of 4T1 tumor-bearing mice was also conducted as above. However, some 4T1 tumor-bearing mice died in the middle stages of experiments. The remaining mice were sacrificed 8 days post-injection.

Histopathology and Immunohistochemistry. To further explore the anticancer mechanisms of PTT and PDT, and their synergistic effect, the excised tumors or scabs were processed into sections that were stained with hematoxylin and eosin (HE) as in our previous research.[37] Briefly, the excised tissues were fixed with 10% formalin solutions and embedded in paraffin. Sections 5-mm thick were made, HE stained, and observed under a microscope. Moreover, the tissue sections were dewaxed, rehydrated, and washed with phosphate buffer solutions (PBS), and endogenous peroxidase was inactivated with 3% hydrogen peroxide (H_2O_2) for 15 min at room temperature. S100 and CD31 in the tissues were measured with the measurement kits (Wuhan GoodBio Technology Co., Ltd., China) according to the instructions.[38-39] The sections were examined under a microscope. Apoptosis assay was also performed as in our previous research.[38-39] Briefly, a TUNEL (Roche, Switzerland) assay method was performed on the sections and incubated for 1 hour at 37 °C. They were incubated with 4',6-diamidino-2-phenylindole (DAPI) for 10 min at room temperature to detect nucleoli after PBS washing. Images of TUNEL and DAPI fluorescence were recorded using a fluorescent microscope.

Statistical Analysis. The results were calculated statistically using the SPSS 16.0 software. All the data was expressed as mean ± standard deviation (SD). One way analysis of variance (ANOVA) with the LSD test was used to identify differences (p<0.05 or p<0.01) between the data.

RESULTS AND DISCUSSION

Characteristics and Photostability of DCC. DCC was a dark green solid and its structure was proved by ^{1}H NMR (**Figure S2** in the supporting information). It has a rigid structure compared to ICG (**Figure 1A**). The DCC solution in methanol exhibited a maximal visible absorption wavelength at 830 nm (**Figure 1B**). The long absorption wavelength was likely to enhance the biological penetration depth of light and decrease the interference of Raman scattering, favoring phototherapy in the body.[40-41] More importantly, DCC had strong photostablility with long photobleaching time. Only 35% reduction of the maximal absorbance of DCC solutions occurred after 830 nm and 250 mW/cm^2 irradiation for 32 min (**Figure 1C**), indicating a remarkable resistance to photobleaching. Hence, DCC could stay stable after long-term light irradiation in the next photothermal treatment.

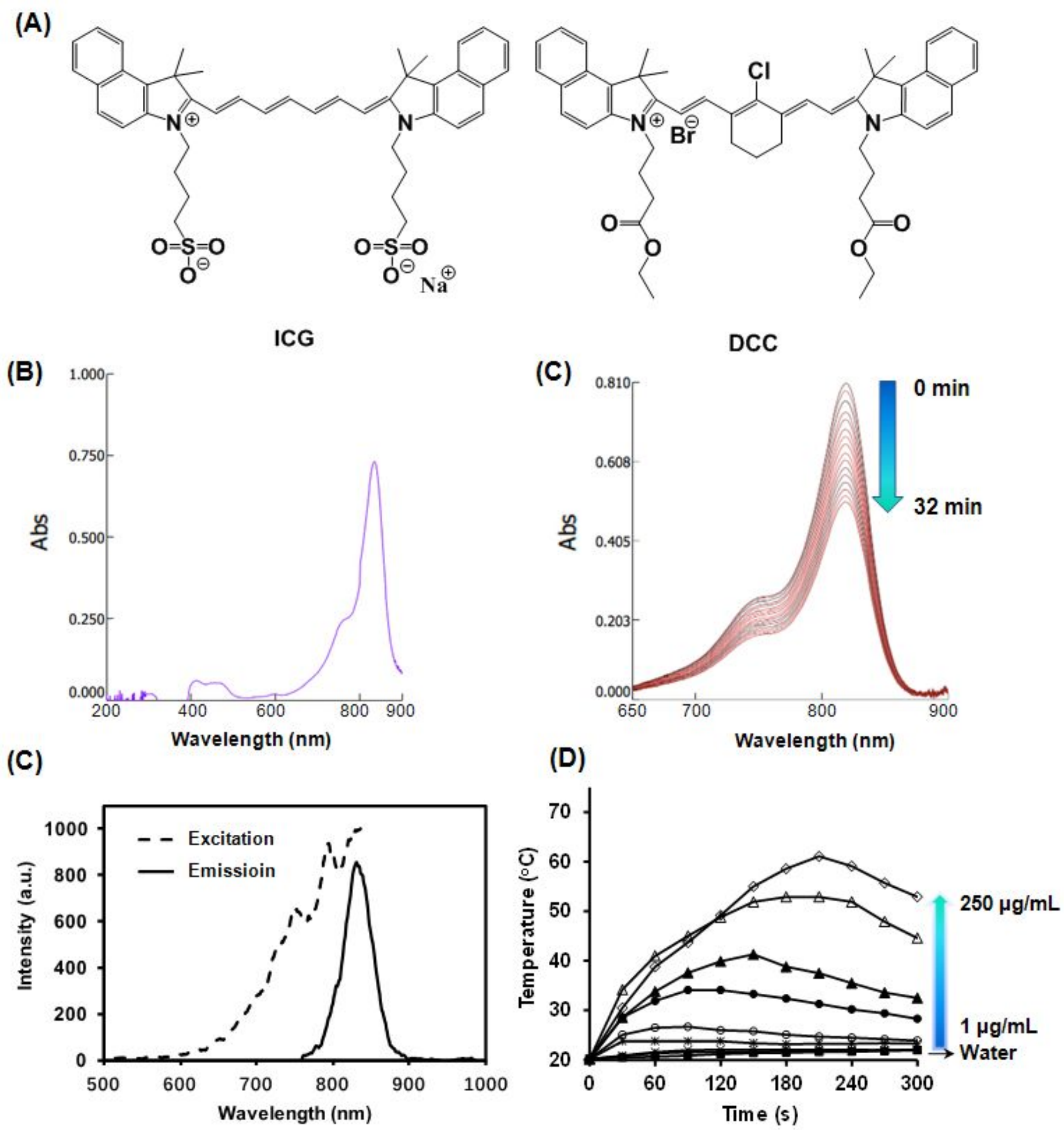

Figure 1. Molecular structures of ICG and DCC (A), and properties of DCC. (B) the UV-vis spectrum of DCC solutions in methanol. (C) Visible absorption spectral changes of DCC solutions in methanol with time dependency. (D) Fluorescent excitation and emission spectra of DCC solutions in DMSO. (E) Temperature profiles of DCC aqueous suspensions after 830 nm and 1.0 W/cm^2 light irradiation with concentration dependency.

Fluorescent Spectra and Fluorescence Quantum Yield of DCC. The fluorescent spectrum of DCC solutions in DMSO exhibited a maximal emission wavelength of 830 nm under the excitation at 750 nm while its excitation spectrum covered a range from 610 nm to more than 810 nm with the peaks at 750 and 794 nm (**Figure 1D**). The 750-nm laser was selected to excite DCC because no emission lights appeared at this wavelength. The fluorescence quantum yield ($\Phi_{F/DCC}$) of DCC in DMSO was 0.28, whereas ICG just had a much lower fluorescence quantum yield of 0.12 than that of DCC. The fluorescence quantum yields of photosensitizers were related to their chemical structures. In general, the rigid structure in the molecule would likely increase its fluorescence quantum yield.[42] Compared to ICG, a major molecular feature of DCC is a rigid bridge ring that is the reason of the high fluorescence quantum yield. Therefore, DCC had much stronger fluorescence emission ability than the clinically applied fluorescence imaging agent, ICG. The long fluorescent emission spectral wavelengths and high fluorescence quantum yield of DCC suggested that DCC would become a promising fluorescence imaging agent.

Strong Photothermal Effect of DCC. Light irradiation remarkably increased the temperature of DCC aqueous suspensions in a concentration-dependent manner (**Figure 1E**). The temperature of a 50 µg/mL DCC suspension rapidly increased from 20 °C to 41.3 °C with a 21.3 °C increase following 150 s light irradiation at 830 nm and 1.0 W/cm^2, while the temperature of the irradiated water hardly changed. Therefore, DCC had the strong photothermal effect with high temperature above 40 °C after a short time irradiation. However, a little decrease of temperature happened in the late stages. In the above case, long-time irradiation would leave to temperature decreasing. For example, after 300-s irradiation, the temperature of solutions decreased from the top of 41.3 °C to 32.5 °C, i.e., 41% temperature decreasing. The experiments were conducted in winter and the room temperature was about 20 °C. Therefore, the heat loss to the environment could not be neglected. In the other cases, the maximal temperature points of DCC suspensions depended on concentrations and the heat loss was unavoidable (**Figure 1E**, **Figure S3**). An appropriate concentration (100 μg/mL DCC) of DCC@PDCZP and the 830 nm irradiation time of 3 min were selected for the *in vivo* pharmacodynamic study. Hyperthermia would lead to irreversible damage to the subjected cells, such as cancer cells,[43] so that the strong photothermal effect of DCC would benefit the treatment of cancer.

Characteristics of PDCZP. PDCZP is a star-shaped copolymer with a zinc phthalocyanine core and four long arms (**Figure 2A**). Its solution in THF had the maximal absorption wavelength of 673 nm (**Figure 2B**), while the solution in DMF had the maximal fluorescent excitation wavelength of 666 nm and the maximal emission wavelength of 681 nm (**Figure 2C**). The fluorescence quantum yield ($\Phi_{F/PDCZP}$) of PDCZP was 0.25, a little lower than that ($\Phi_{F/ZnPc}$, 0.30) of its parent photosensitizer, ZnPc. The singlet oxygen quantum yield (Φ_{PDCZP}) of PDCZP was 0.47, close to that (0.41) of another PDCZP analogue (PEG_{2000}-PDCZP), and a little lower than that (0.56) of its parent ZnPc and that (0.64) of another amphiphilic derivative of ZnPc (ZnPc-Brij 58 conjugate, ZPB) previously prepared in our lab.[31, 44] The long PDC chains of PDCZP might shield energy transportation or oxygen diffusion, leading to a decrease of Φ. PDCZP formed a nanoscale particle in water with a mean hydrodynamic size of 60 nm and a polydispersive index (PDI) of 0.264.

PDCZP was positively surface-charged in water (neutral, about pH 7) with the zeta potential of 18.57 mV due to its amine-contained pDEA chains.

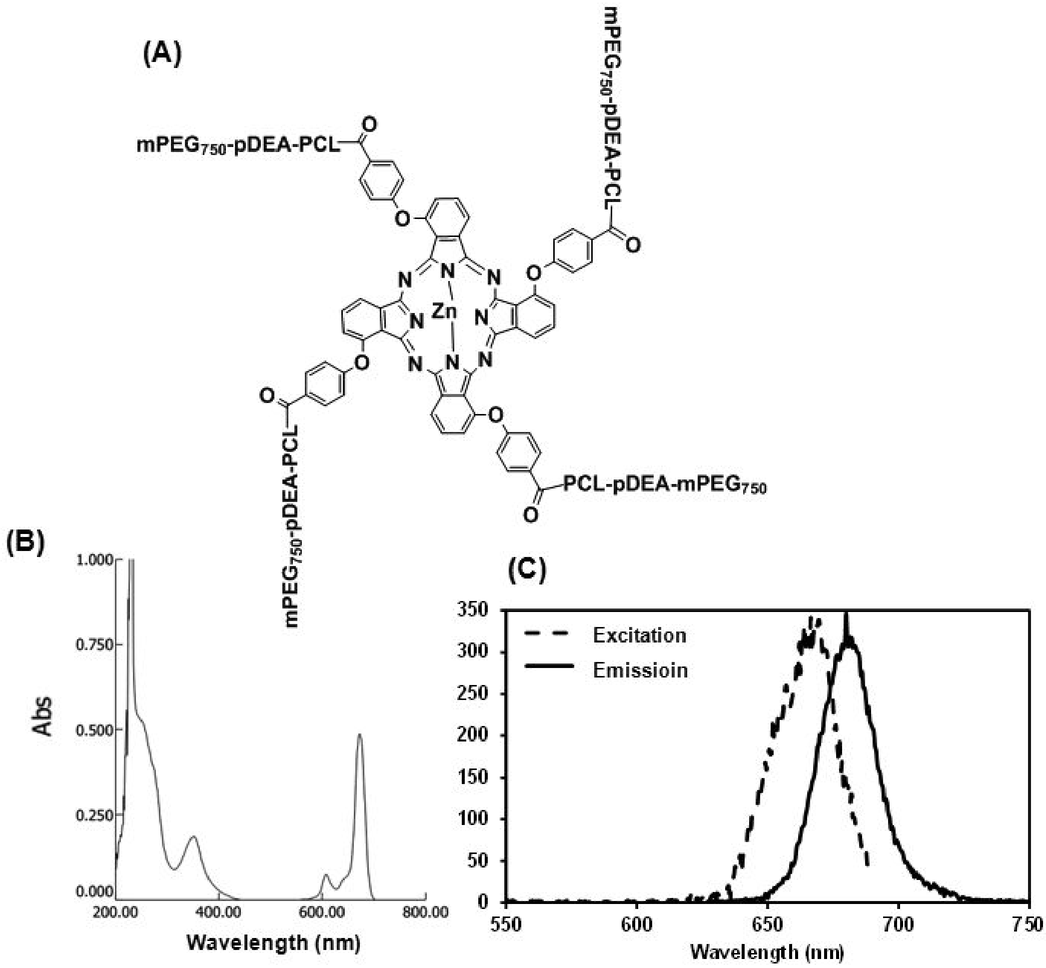

Figure 2. Properties of PDCZP. (A) Molecular structure of PDCZP. (B) The UV-vis absorption spectrum of PDCZP solutions in THF. (C) Fluorescent excitation and emission spectra of PDCZP solutions in DMF.

Design and Preparation of DCC@PDCZP. PDCZP is a pH-sensitive copolymer nanocarrier, prepared by us and reported previously.[31] Doxorubicin was loaded in the nanocarriers that expressed the significant *in vivo* anti-tumor treatment based on their long-circulating and pH-sensitive properties after i.v. administration.[31] Moreover, the pH-sensitive property of PDCZP benefits not only the pH-responsive release of drugs in tumors but also the stable entrapment of drugs. Here, we used PEG 750 to replace previous PEG 2000 to prepare PDCZP because the short PEG chains were satisfied for preventing the nanocarriers from aggregation with high stability. The pH-sensitive chain, i.e., pDEA, did not change in this study because its high pH-sensitive property had been confirmed in our previous research.[31, 45-46] Moreover, the DCC@PDCZP was i.t. injected in this study, leading to the nanocarriers directly exposed to the low pH environment of tumors and the pH-responsive merit well expressed.

The injection method was used for preparation of DCC@PDCZP that appeared as a homogeneously dark green solution that remained unchanged in appearance within several days at room temperature. Unlike the usually applied injection method,[31] here water was slowly injected into the DCC/PDCZP solution in THF. This preparation process could gradually make the whole system changing from a organic phase state to a water phase state so that DCC molecules might have sufficient time and space to enter the hydrophobic core of PDCZP nanocarriers. DCC@PDCZP composed of 1:2 (w/w) DCC/PDCZP had the relatively high EE (65.9%) and LE (25.6%).

pH-Responsive Properties of DCC@PDCZP. The pH-response of anticancer agent-loaded nanocarriers was expected to facilitate the quick release of the loaded drugs at the tumor tissues due to low pH.[47] PDCZP has been proved to be a pH-responsive nanocarrier in our previous work.[31] Here DCC@PDCZP also showed some pH-responsive properties involving size, zeta potential and DCC release (**Figure 3A, 3B**). The pH-sensitive pDEA chain in PDCZP was responsible for this response.[31, 45-46] The lower the pH was, the larger DCC@PDCZP became. Its mean size was 126.6, 96.76 and 68.07 nm at pH 5.0, 6.5 and 7.4, respectively (**Figure 3A**). The change of sizes was also shown by TEM (**Figure 3A**). Interestingly, DCC@PDCZP was positively stained by sodium phosphotungstate at low pH due to the positive surface charge, where the strong absorption of phosphotungstate on the surface of PDCZP led to an apparently large size. Furthermore, the surface charge of DCC@PDCZP changed from the positive zeta potential of 44.2 mV and 28.9 mV at pH 5.0 and 6.5 to the negative zeta potential of −17.9 mV at pH 7.4 (**Figure 3A**).

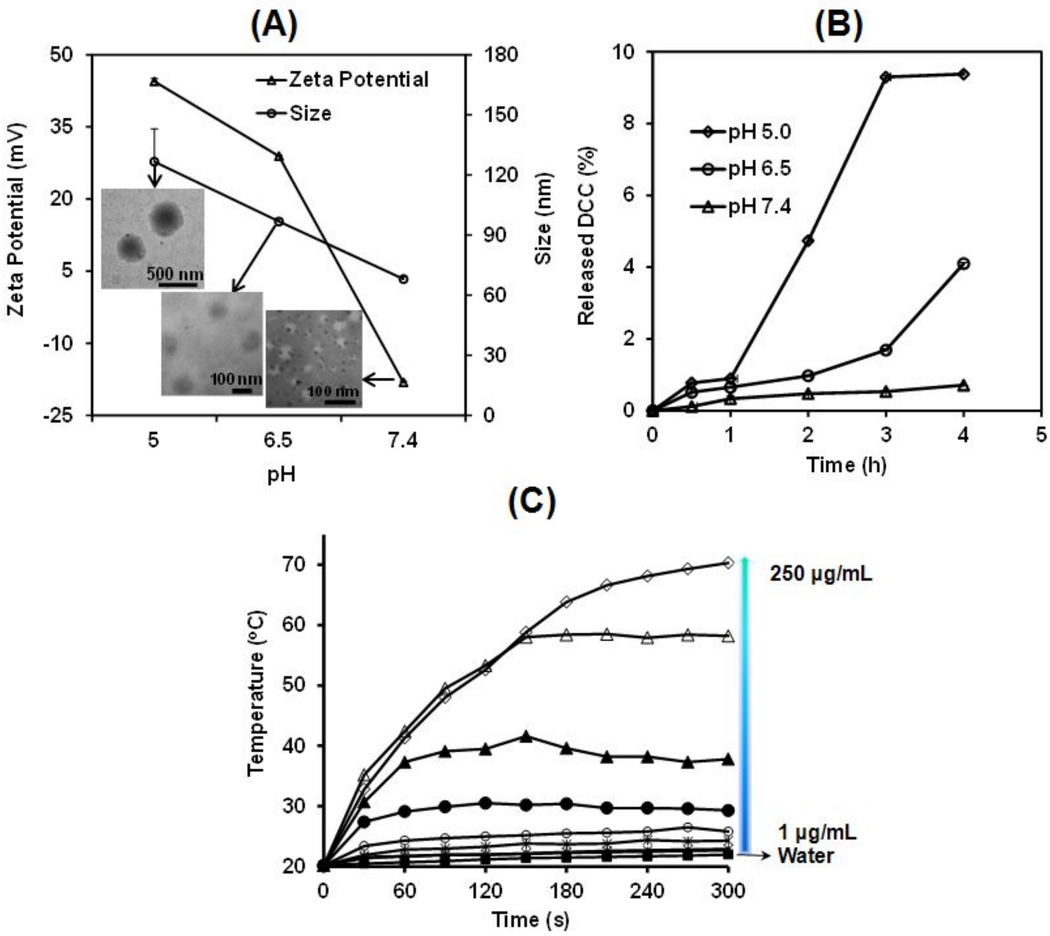

Figure 3. Properties of DCC@PDCZP. (A) Size and zeta potential of DCC@PDCZP and the corresponding TEM images with pH dependency (n = 3). (B) DCC release from DCC@PDCZP with pH dependency (n = 3). (C) Temperature profiles of

DCC@PDCZP suspensions after 830 nm and 1.0 W/cm^2 light irradiation with concentration dependency.

DCC@PDCZP is positively-charged at the low pH environment of tumor tissues so that it could be likely to interact with surrounding cancer cells as i.t. injection of these carriers. Moreover, once DCC@PDCZP was internalized into the endosomes and then lysosomes that were generally at pH 5.0 or lower, its highly positive charge state (i.e., 44.2 mV) would lead to the so-called “proton sponge” effect and then membrane damage of lysosomes and cargos release to cell plasma,[48] favoring subsequent PTT and PDT.

DCC release from DCC@PDCZP was also highly dependent on pH (**Figure 3B**). pH 7.4, 6.5 and 5.0 may represent the environments of blood circulation and normal tissues, tumor tissues and cellular lysosomes, respectively.[49] Here DCC release from DCC@PDCZP was very little at pH 7.4, but highly improved at pH 6.5 and 5.0, favoring the treatment of cancer. Our previous studies and other reports showed a similar conclusion.[31, 45-46] More importantly, unlike other research, we performed the i.t. injection of DCC@PDCZP directly into tumor tissues so that little drug was wasted.

High Photothermal Effect of DCC@PDCZP. DCC@PDCZP showed the similar photothermal behavior to DCC, also depending on time and concentrations (**Figure 3C**). For example, a 50-μg/mL DCC@PDCZP suspension underwent a rapid increase of temperature from 20 °C to 41.6 °C after 150-s light irradiation at 830 nm and 1.0 W/cm^2 and then a little decrease to 37.8 °C after 300 s irradiation. Other

DCC@PDCZP suspensions of different concentrations also showed similar profiles (**Figure S4**). However, there was a special case. A 250 μg/mL DCC@PDCZP suspension maintained a profile of continual temperature increase despite the long time irradiation for 300 s. Therefore, unlike free DCC, DCC@PDCZP maintained high temperature for a long time post-irradiation, which might be attributed to PDCZP-self hindrance of thermal diffusion or heat loss. The long-term maintenance of hyperthermia should favor ablation of tumors.

No Hemolysis by DCC and DCC@PDCZP. Neither free DCC nor PDCZP showed any hemolysis within 3 hours after incubation with erythrocytes even when the concentration of DCC or PDCZP was up to 5 mg/mL. All these samples' supernatants showed nearly zero absorbance at 577 nm. Therefore, DCC@PDCZP had no hemolytic effect and the safety of its injection was ensured. The results of hemolytic experiments were shown in **Figure S5**, **Table S1** and **Table S2** in the supporting information.

High Dark Cytotoxicity of DCC and Little Dark Cytotoxicity PDCZP. We detected the effect of light irradiation on the growth of mouse melanoma B16-F10 cells and mouse breast cancer 4T1 cells. The light irradiation, including 830 nm (1 W/cm^2) and 660 nm (200 mW/cm^2), did not affect the growth of the two types of cells even though the irradiation time was extended to 5 min. The cells always kept a high viability of more than 95%. Dark cytotoxicity of the photosensitizer PDCZP, the photothermal agent DCC and the anticancer chemotherapeutic mitoxantrone was also investigated. Mitoxantrone is a synthetic anthraquinone chemotherapeutic drug that can intercalate with DNA to inhibit their synthesis and transcription. Mitoxantrone is used to treat certain types of cancer, including breast cancer and melanoma. The *in vitro*/*in vivo* anti-melanoma effect of mitoxantrone was reported a lot.[50-53] B16-F10 cells showed different viability depending on the types and concentrations of regimens (**Figure 4A**). The half inhibitory concentrations (IC_{50}) of PDCZP, DCC and mitoxantrone under darkness were 409, 10.3, and 1.46 μg/mL, respectively. Therefore, PDCZP had hardly any dark cytotoxicity, while DCC and mitoxantrone had a relatively strong dark cytotoxicity though the effect of mitoxantrone was higher (Figure 4A). However, these values were obtained at 24 hours post-incubation. In fact, DCC could not maintain a high concentration for such a long time at the *in vivo* targeted site. Therefore, the dark incubation time was further investigated for DCC and DCC@PDCZP.

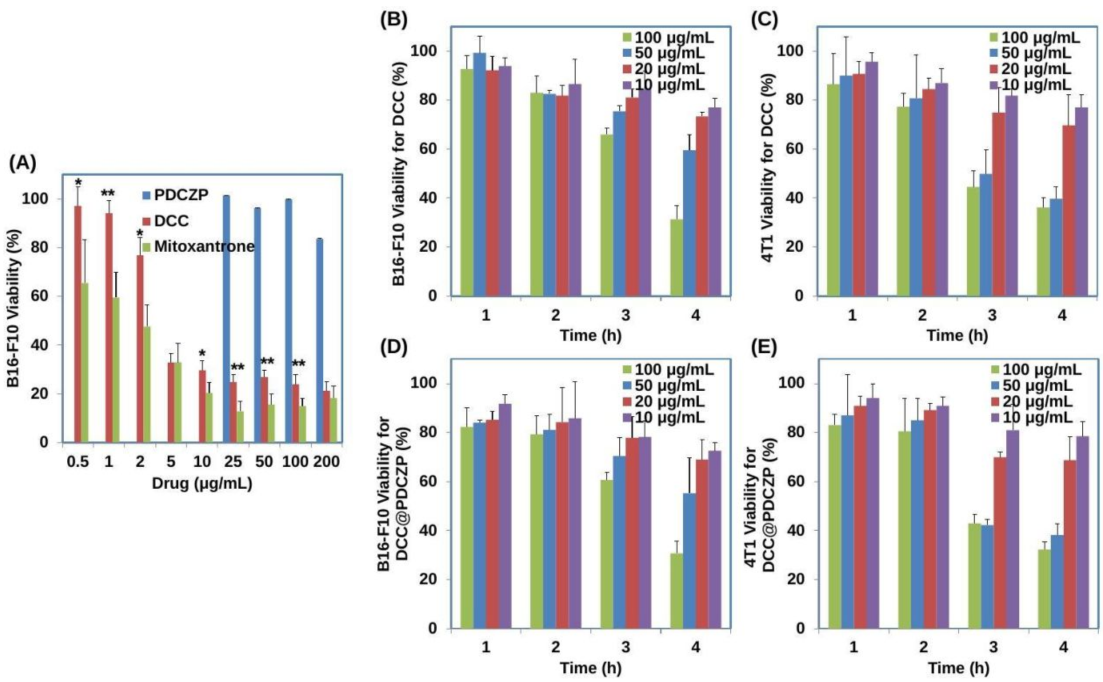

Figure 4. Dark cytotoxicity of PDCZP, DCC and mitoxantrone on B16-F10 cells depending on concentration (A), and DCC and DCC@PDCZP on B16-F10 (B, D) and

4T1 cells (C, E) depending on time and concentration. The dark cytotoxicity of DCC and mitoxantrone was compared (A). $N = 4$, * $p < 0.05$, ** $p < 0.01$.

Both DCC and DCC@PDCZP showed the similar dark cytotoxicity on B16-F10 and 4T1 cells (**Figure 4B−E**). Two hours post-incubation, the viability of all the cells was close to or above 80%, even with highly concentrated DCC (e.g., 100 μg/mL). However, the growth of cells was highly inhibited by the highly concentrated samples at 3 hours post-incubation, such as 100 μg/mL DCC, and the cell viability was only less than 50%. Therefore, phototherapy should be initiated at 2 hours post-dark incubation.

High *In Vitro* Anticancer PDT/PTT Effect of DCC@PDCZP. The *in vitro* anticancer PDT/PTT effect of DCC@PDCZP was explored in depth on B16-F10 and 4T1 cells. Compared to the regimens under darkness, the therapeutic effect was highly enhanced by both the PDT of PDCZP at 2 hours post-incubation and the PTT of DCC, and more importantly, the synergistic PDT/PTT of DCC@PDCZP (**Figure 5**). Moreover, the synergistic PDT/PTT effect of DCC@PDCZP was always the highest one among all the groups at various concentrations. Even at a low concentration of 20 μg/mL DCC, DCC@PDCZP still showed a high cytotoxicity with the cell viability of less than 30% under light irradiation, whereas the PTT of DCC showed the cell viability just close to 70% at the same concentration (**Figure 5**). The IC_{50} of PDCZP under 660 nm irradiation and DCC@PDCZP under 830 nm irradiation was 46.13 μg/mL and 41.42 μg/mL for B16-F10 cells, respectively. However, the IC_{50} of DCC@PDCZP under 830 nm/660 nm irradiation was as low as 7.92 μg/mL. The cytotoxicity on 4T1 cells was similar to that of B16-F10 cells. The synergistic effect could be ascribed to the PTT-triggered disruption of lysosomal membranes and thus enhanced accessibility of photosensitizers to target organelles. The enhanced accessibility is critical to the therapeutic index of photosensitizers since singlet oxygen has a very short half-life and limited diffusion range in the biological system.[54]

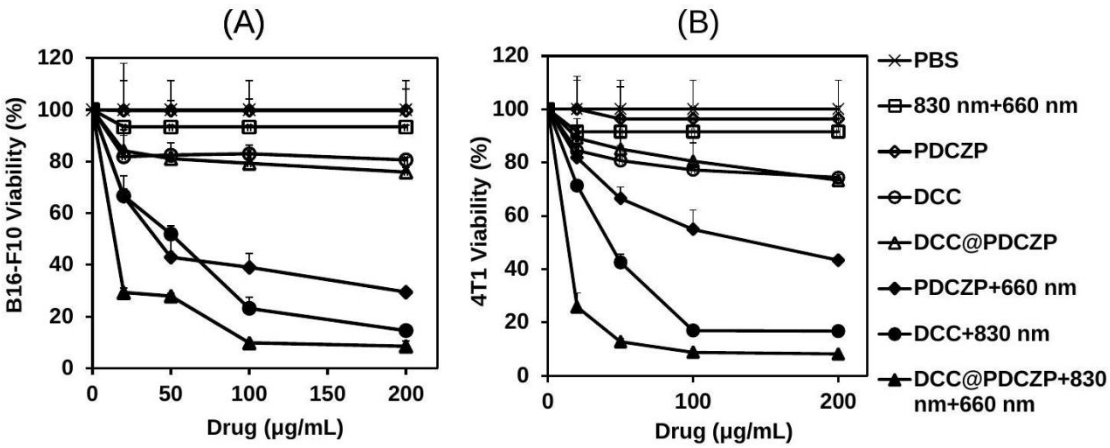

Figure 5. *In vitro* anticancer effect of PDCZP, DCC and DCC@PDCZP on B16-F10 (A) and 4T1 cells (B) under/without 830 nm or/and 660 nm irradiation in comparison with the controls (PBS and 830 nm/660 nm irradiation) (n = 3).

Highly Efficient Cellular Uptake of PDCZP and Its Localization in Cells. The sufficient cellular internalization of DCC@PDCZP would enhance the PDT/PTT effect. The flow cytometric result showed that FITC@PDCZP was rapidly internalized into the B16-F10 cells (**Figure 6A**). High uptake efficiency was shown within 8 hours and the fluorescence hardly changed after 4 hours. Therefore, light irradiation was initiated at 4 hours post-injection of regimens in the next *in vivo* experiment. Moreover, the internalized DCC amount of DCC@PDCZP was about 3 times that of free DCC that may form precipitates when mixed with the culture media

(**Figure 6B**), leading to low endocytic efficiency. Therefore, DCC, as a hydrophobic photothermal agent, had to be formulated into a nanocarrier, i.e., PDCZP, before injection into animals.

The localization of DCC@PDCZP after internalization into 4T1 cells was investigated by CLSM. There was larger green fluorescence area (representing PDCZP) than the red area (representing lysosomes) in the merged images (**Figure 6C**), indicating that some DCC@PDCZP nanocarriers could escape from the lysosomes due to the so-called "proton sponge effect".[55] The amine groups of PDCZP can capture hydrogen protons in the lysosomes after internalization, leading to rapid increasing of the osmotic pressure and then the rupture of some lysosomes to release PDCZP to the cellular plasma. Moreover, after irradiation, some red fluorescence areas diminished (**Figure 6D**), indicating some lysosomes were destroyed due to the photothermal effect of DCC. The lower cell density in **Figure 6D** than that in **Figure 6C** could further demonstrate some cells were damaged by heat produced by the photothermal effect.

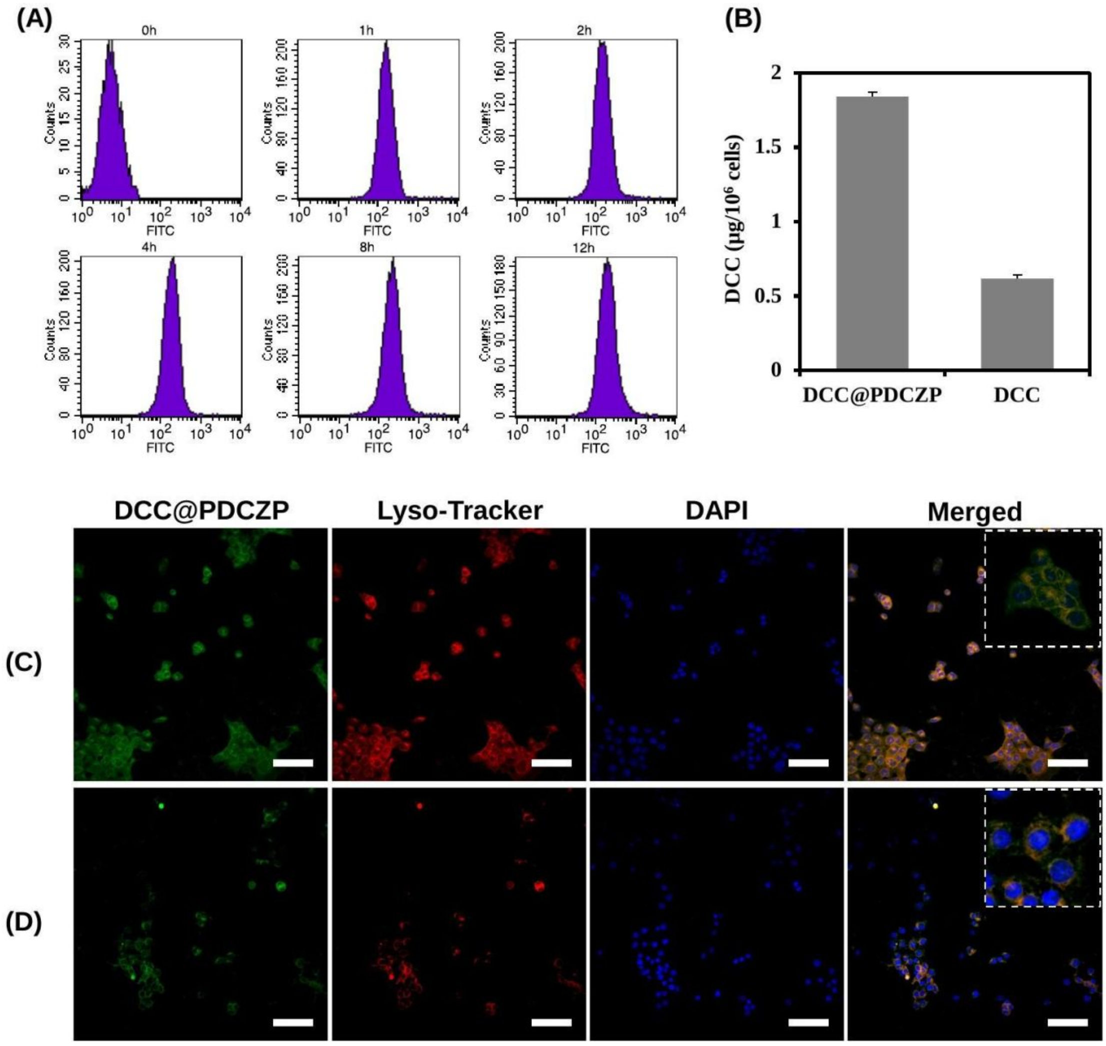

Figure 6. Cellular uptake and localization of PDCZP nanocarriers. (A) Cellular uptake proved by the flow cytometry of FITC@PDCZP in B16-F10 cells. (B) The DCC amount in B16-F10 cells after incubation with DCC@PDCZP (n = 4). PDCZP localization in 4T1 cells shown by the confocal laser scanning microscopy without 830 nm light irradiation (C) or with the irradiation (D) after incubation with DCC@PDCZP. The inserted enlarged images in the merged images of Graphs (C) and (D) show the details. The scale bars mean 100 μm.

Enhanced Imaging of Tumors by DCC@PDCZP. DCC showed a long excitation wavelength besides its high photothermal efficiency. The B16-F10 tumor showed significant infrared thermal imaging when the tumor was irradiated by 830 nm laser, where the surface temperature of the tumor increased to 60.4 °C (**Figure 7A-a**). The rich melanin in the melanoma can absorb the light that is translated to heat.[56] This phenomenon is actually applied in non-invasive cutaneous melanoma diagnosis.[57-58] Infrared thermal imaging and high temperature were also shown when DCC@PDCZP was i.t. injected into the melanoma (**Figure 7A-b**). For 4T1 tumor that had no sufficient melanin, the thermal imaging effect of i.t. DCC@PDCZP was still significant with the tumor surface temperature of 45.3 °C while the irradiation treated tumor expressed a surface temperature of only 37 °C, with a little increase from the normal skin temperature of 35 °C (**Figure 7A-c, d**).

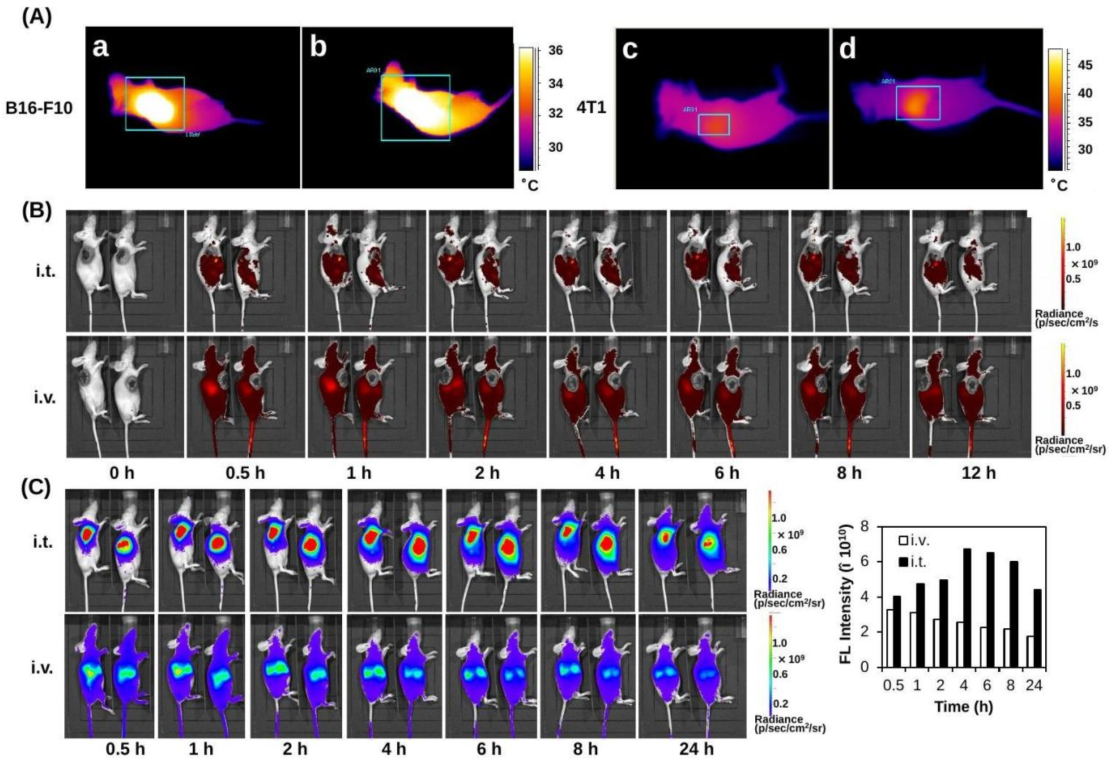

Figure 7. Imaging of tumors. (A) Thermal imaging of B16-F10 tumors without (a) or with (b) i.t. injection of DCC@PDCZP, and 4T1 tumors without (c) or with (d) the injection. (B) Fluorescence imaging of B16-F10 tumors after i.t. or i.v. injection of DCC@PDCZP at different time points. (C) Fluorescence imaging of 4T1 tumors after

i.t. or i.v. injection of DCC@PDCZP at different time points, and the fluorescence (FL) intensity, where the FL intensity was the mean from two mice.

Fluorescence imaging showed the difference of DCC *in vivo* distribution in the tumor-bearing mice between i.t. and i.v. injection of DCC@PDCZP (**Figure 7B, 7C**). The i.v. injection caused DCC to be mainly distributed in the liver, resulting from the phagocytosis of DCC@PDCZP by the Kupffer cells of the liver. However, no liver distribution of DCC was found after the i.t. injection. Surprisingly, there was no fluorescence at the melanoma site (**Figure 7B**), possibly resulting from the strong light absorption of melanin in the melanoma tissues. 4T1 tumors had little melanin so that the tumor always maintained strong fluorescence intensity even at 4 hours post-i.t. injection (**Figure 7C**). We selected this time point to initiate light irradiation. The above results demonstrate that the i.v. injected PDCZP-like nanoparticles can hardly target tumors. Hence, the strategy of i.t. injection may promise a good solution to the tumor targeting problem in the terms of time and space, especially for superficial tumors.

Ablation and Little Recurrent Efficiency of Melanoma by DCC@PDCZP under Light Irradiation.

Experimental design of pharmacodynamic study. A series of regimens, including DCC and PDCZP alone, and negative and positive control agents (i.e., PBS and mitoxantrone), were compared with DCC@PDCZP, wherein all the conditions including light irradiation and darkness were thoroughly considered. Light irradiation was initiated at 4 hours post-i.t. injection. Considering the strong photothermal effect of melanoma-self under 830 nm irradiation and then damage of tumors, the mice in Groups f−i were merely injected only once with light irradiation while the mice in Group a−e were injected four times without irradiation.

Phototherapeutic effect. The very strong photothermal effect was shown in Groups g−i due to DCC and/or melanin, leading to seriously burned wounds at the tumor sites. Edema appeared on Day 2 and then scabs were formed on Day 3. In the following days, the tumor tissues in the DCC-contained Groups g and h continually shrank and the tumors were smaller compared to the other groups (**Figure 8A, 8B**). From Day 7, no tumor tissues were seen in Group h with DCC@PDCZP under 660/830 nm irradiation although only a small number of scabs remained (**Figure 8C**). By contrast, recurrent melanomas appeared around the scabs in all the mice of Group i (light irradiation alone) from Day 5 and then grew quickly (**Figure 8B**). Furthermore, only one mouse had recurrent melanoma around the scab in Group g with DCC under irradiation. In Groups c−f, significant anti-melanoma effect was also shown compared to the negative control (Group a), but the effect was much weaker than that in Groups g−i. Groups g and i had the similar tumor weight (p = 0.092) (**Figure 8D**), indicating that melanoma-self also had strong PTT effect. Therefore, PTT played a key role in the local treatment of melanoma. More importantly, the combination of PTT/PDT could effectively inhibit the recurrence of melanoma besides ablation of the tumors. The final resected tumors and corresponding tumor weight further demonstrated the above conclusion (**Figure 8B, 8D**).

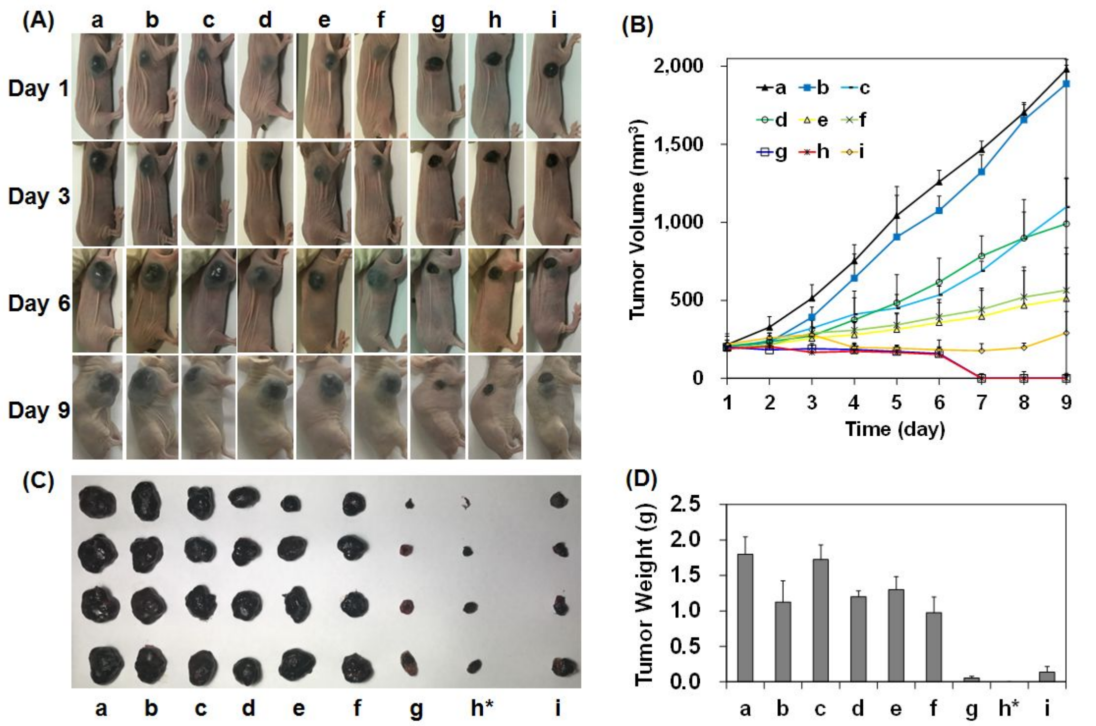

Figure 8. Pharmacodynamic effect of regimens on B16-F10 melanoma. (A) Appearance of tumor-bearing mice at the end of therapy. (B) Tumor volume. (C) Appearance of excised tumors. (D) Tumor weight. Groups a−i included the mice treated with PBS (a), PDCZP without irradiation (b), DCC without irradiation (c), DCC@PDCZP without irradiation (d), mitoxantrone (e), PDCZP under 660 nm irradiation (f), DCC under 830 nm irradiation (g), DCC@PDCZP under 830 nm and then 660 nm irradiation (h), and 830 nm and then 660 nm irradiation (i), respectively. Moreover, Group g and h had no significant tumor tissues from Day 7. Scabs remained in the sites of tumors so that the possible tumor sizes could not be measured. The apparent "0" values are set in Figure 8B for Groups g and h. Group h* in Graphs (C) and (D) indicated no tumor tissues, where the black tissues shown in Group h* were actually scabs after ablation of tumors. Photothermal effect also happened in Groups g and i, although some recurrent melanomas appeared around the scabs at different time. In Graph (D), the tumor weight of Groups g and i was compared with $p = 0.092$ and $n = 4$.

PTT can eradicate tumors with photothermal agents such as ICG, gold nanoparticles, $(NH_4)_xWO_3$ nanocubes, etc.[59-61] However, the recurrence of tumors had not been reported with PTT. In this study, we proved that just PTT (Groups g and i) eradicated melanoma but recurrence was still unavoidable, possibly resulting from a little residual cancer cells as the seeds of recurrence. In contrast, no tumor recurrences were shown at the end of therapy after the combination of PDT/PTT by i.t. injection of DCC@PDCZP, suggesting the strong synergistic effect of PDT/PTT. In this study, a sequential PDT following PTT could initiate a second attack against the residual cancer cells by singlet oxygen. Finally, all the cancer cells could be eventually eliminated by the programmable combination of PTT/PDT with i.t. injected DCC@PDCZP.

Highly Efficient *In Vivo* Anti-Breast Cancer Effect of DCC@PDCZP under Light Irradiation. 4T1 cells lead to highly metastatic mouse breast cancer.[62-63] As in the above melanoma therapy, the same regimens were also applied to the treatment of 4T1 breast cancer with or without light irradiation. Under light irradiation, DCC and DCC@PDCZP (Groups g and h) had strong PTT effect on 4T1 tumors. Significant burned wounds appeared and then scabs were formed (**Figure 9A**). However, unlike melanoma, 4T1 tumors had little melanin so that merely 830 nm irradiation did not induce hyperthermia. On Day 3, one mouse died in Group a with PBS. On Day 4, one mouse was dead in Groups b and i with PDCZP and light irradiation alone (**Figure 9E**). On Day 5, only scabs remained in Group h, whereas a little of the recurrent tumor tissues appeared around the scabs in Group g with DCC under irradiation. We assumed that the tumors had been eradicated in Group h; and more importantly, there was little recurrence in the original place at this time (**Figure 9B−D**). The tumor weight of Groups e, g and i was compared. Significant difference ($p < 0.05$) was shown between Groups e and i and very significant difference ($p < 0.05$) was shown between Groups g and i (**Figure 9D**). Therefore, the anti-breast cancer effect of local PTT alone was stronger than that of mitoxantrone and much stronger than that of PDT alone. Unlike the above melanoma therapy, light irradiation alone did not show any anti-breast cancer effect (see Group i in **Figure 9**). Moreover, the synergistic advantage of combinational PTT/PDT was well expressed again (see Group h in **Figure 9**). However, one mouse was also dead in Groups g and h (**Figure 9E**), possibly resulting from the rapid metastasis of 4T1 breast cancer. The 4T1 breast cancer is a metastatic tumor with a high mortality. Mitoxantrone is a potent anticancer chemotherapeutic, which may distribute in the whole body even after local administration. Therefore, mitoxantrone was administered once every two days and it may have therapeutic effect for the metastasis of 4T1. However, according to the experiment results, here the combinational PTT/PDT may be suitable for the non-metastatic tumors because its effect is limited to the local sites.

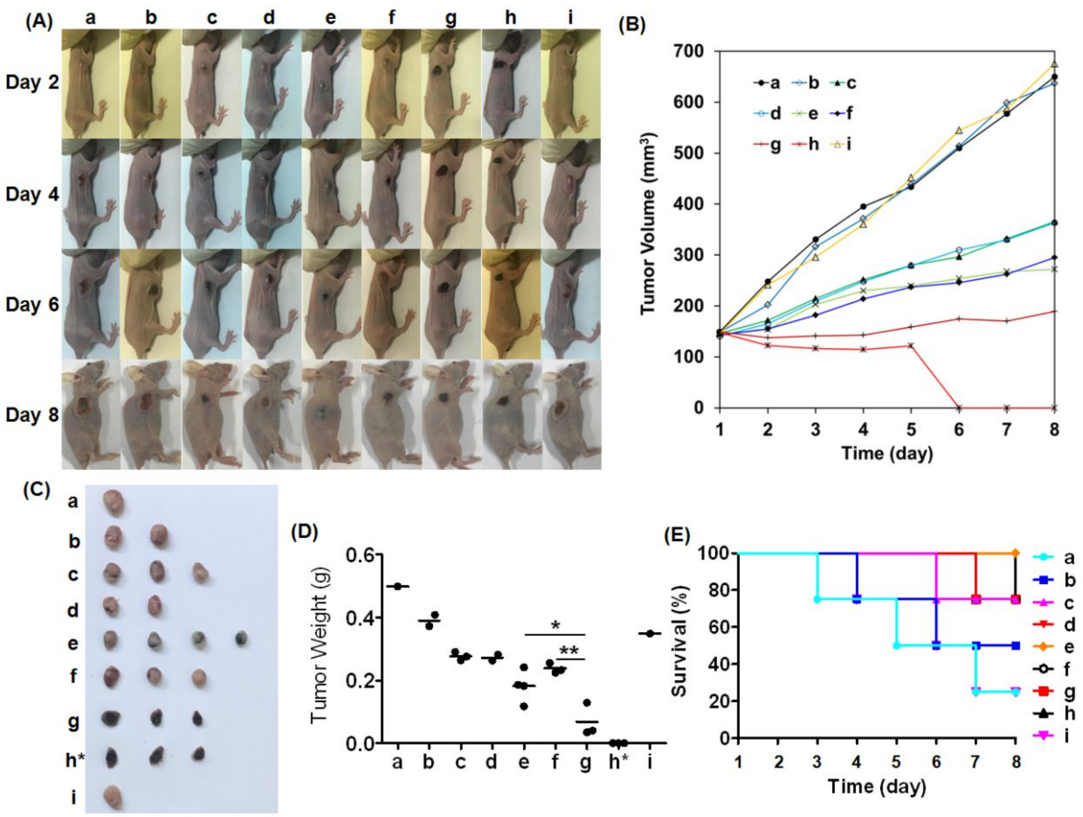

Figure 9. Pharmacodynamic effect of regimens on the 4T1 breast cancer of mice. (A) Appearance of tumor-bearing mice at the end of therapy. (B) Tumor volume. (C) Appearance of excised tumors. (D) Tumor weight. (E) Survival curves. The meanings of Groups a–i are referred to Figure 8. Group h* in Graph (C) and (D) indicated no tumor tissues, where the black tissues were actually scabs after ablation of tumors due to the potent PTT effect of DCC@PDCZP. Photothermal effect also happened in Group g, although some recurrent tumor tissues appeared around the scabs. In Graph (D), the tumor weight of Groups e, g and i was compared. * $p < 0.05$; ** $p < 0.01$; n = 1-4.

Anticancer Mechanisms of PDT and PTT. In the pharmacodynamic study of melanoma, HE staining showed that the excised tissues in Group h with DCC@PDCZP/irradiation had heavy cancer cell necrosis with few cancer cells and little extensive hemolysis (**Figure 10A**). By contrast, a large number of cancer cells appeared in Groups a and b. The treatments of DCC and DCC@PDCZP under darkness (Groups c and d) led to necrosis of some cancer cells due to the dark toxicity of DCC. The PDT of PDCZP and the PTT of DCC under irradiation (Groups f and g), and irradiation alone (Group i, also having photothermal effect) showed significant anti-melanoma effect. Moreover, the surrounding recurrent tumor tissues in Group j were full of highly malignant cancer cells.

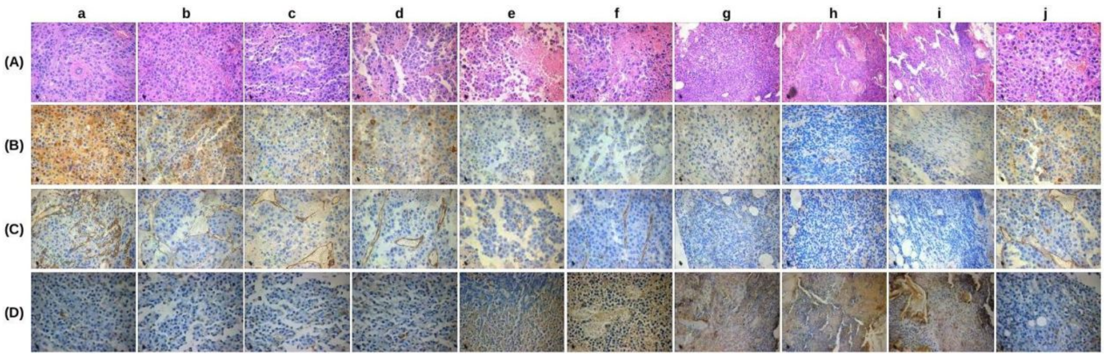

Figure 10. Images of the sections of B16-F10 melanoma tissues and *in situ* scabs. (A) HE stained sections. (B) S100 expressions. (C) CD31 expressions. (D)TUNEL expressions. The meanings of Group a–i are the same as those in the caption of Figure 8. However, the sample in Group j came from the surrounding recurrent tumor tissues of Group i with the treatment of 830 nm and then 660 nm light irradiation.

The expression of S100 proteins is related to the malignancy of melanoma.[64] CD31 expression represents the vigorous growth of tumor neovascularization.[65] The immunohistochemical results showed that S100 and CD31 were hardly expressed in Group h with DCC@PDCZP under irradiation, and only the scabs existed (**Figure 10B**, **10C**). By contrast, the other groups had significant expressions of S100 and CD31. Moreover, the recurrent melanoma, i.e., the surrounding recurrent tumor tissues in Group j also showed the typical feature of melanoma. TUNEL staining indicates cellular apoptosis.[66] Here, all the groups with PTT, involving Groups g, h and i, showed the high TUNEL levels while the levels of the other groups were relatively low (**Figure 10D**). In addition, the group with PDT (Group f) had a high TUNEL level. Other studies also showed the similar results of PDT and PTT. [62, 67-68]

In the pharmacodynamic study of breast cancer, all the results of HE staining, CD31 expression and TUNEL levels were similar to those of the above therapy of melanoma (**Figure 11A**). However, the two therapies had important difference in Group i (light irradiation alone). Unlike melanoma, 4T1 breast cancer cells contained little melanin, so light irradiation alone had no effect on the tumors. The groups with PTT, involving Groups g and h, had high anticancer effect, although Group j (the surrounding recurrent tumor tissues of Group g) showed significant recurrence of tumors with the high CD31 expression and TUNEL levels (**Figure 11B, 11C**). Mitoxantrone also significantly improved the apoptosis of 4T1 cells (Group e, **Figure 11C**), as reported.[69]

In summary, the combination of PTT/PDT, i.e., DCC@PDCZP under light irradiation, had strong anticancer effect on orthotopic melanoma and breast cancer and no local recurrences took place after 8 days post-i.t. injection compared with PTT or PDT alone. The major anticancer mechanisms involve improvement of cancer cell necrosis via hyperthermia, inhibition of local neovascularization, and enhancement of cancer cell apoptosis.

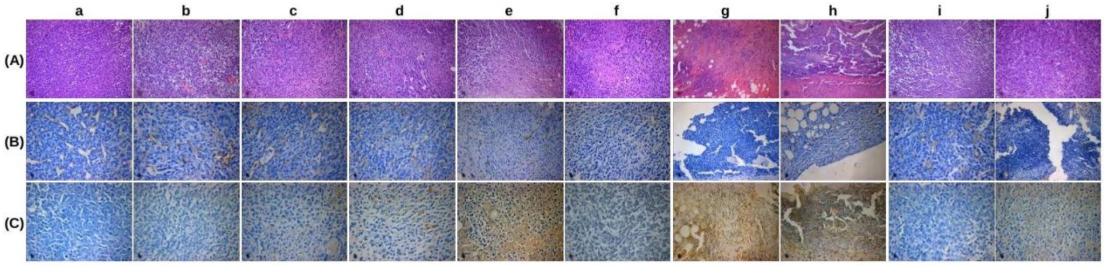

Figure 11. Images of the sections of 4T1 breast cancer tissues and *in situ* scabs. (A) HE stained sections. (B) CD31 expressions. (C) TUNEL expressions. The meanings of Groups a−i are the same as those in the caption of Figure 8. The sample in Group j came from the surrounding recurrent tumor tissues of Group g with DCC under 830 nm irradiation.

CONCLUSIONS

Phototherapy needs light penetrating through the skin. Unfortunately, only the light of long wavelength (e.g., 830 nm) can enter the deep tissues beneath the skin, but only the depth of several micrometers or one centimeter may be achieved. Although the tumor in deep tissues of the body such as brain tumor can be treated with phototherapy through insertion of fiber optics, skin cancers or the tumors under the skin are usually appropriate for phototherapy such as melanoma or breast cancer. Both melanoma and breast cancer are high malignant carcinomas. Surgery, chemotherapy and radiotherapy are the major treatments. These superficial tumors are appropriate to phototherapy due to near-infrared light penetration to the biological tissues. However, the conventional i.v. administration of phototherapeutics leads to low drug distribution in the tumor tissues even though nanocarriers are used. Here, we tried i.t. injection of phototherapeutics and then light irradiation for local treatment of melanoma and breast cancer. We find that the combination of PTT/PDT, i.e., DCC@PDCZP, under 830 nm and 660 nm light irradiation, leads to excellent therapeutic effect. The combinational PTT/PDT not only eradicates the tumors but also hinders local recurrence of tumors within a certain period due to the synergistic effect of PTT and PDT. However, the combinational PTT/PDT may be suitable for the non-metastatic tumors because its effect is limited to the local sites. Furthermore, only one i.t. injection of this PTT/PDT nanoformulation can produce the desired effect for therapy of local tumors. The i.t. injection of PTT/PDT nanoformulations is a highly promising local treatment of superficial tumors.

ASSOCIATED CONTENT

Supporting Information

The Supporting Information is available free of charge on the ACS Publications website at DOI: 10.1021/

Synthetic procedures of DCC, ^{1}H NMR spectrum of DCC, temperature profiles of DCC and DCC@PDCZP depending on concentrations under light irradiation, hemolytic phenomena and data of PDCZP and DCC.

AUTHOR INFORMATION

Corresponding Author

*E-mail: jinyg@sina.com

ORCID

Yiguang Jin: 0000-0002-3528-1397

Notes

The authors declare no competing financial interest.

ACKNOWLEDGEMENT

We thank the National Key Technologies R&D Program for New Drugs of China (grant number: 2012ZX09301003-001-009) for financial support of this work. We are grateful to Prof. Xiansheng Lu for his careful proof-reading.

REFERENCES

1. Devadasu, V. R.; Bhardwaj, V.; Kumar, M. N. Can controversial nanotechnology promise drug delivery? *Chem. Rev.* **2013,** *113* (3), 1686-1735. DOI: 10.1021/cr300047q.

2. Park, K. Facing the Truth about Nanotechnology in Drug Delivery. *ACS Nano* **2013,** *7* (9), 7442-7447. DOI: 10.1021/nn404501g.

3. Danhier, F. To exploit the tumor microenvironment: Since the EPR effect fails in the clinic, what is the future of nanomedicine? *J. Control. Release* **2016,** *244* (Pt A), 108-121. DOI: 10.1016/j.jconrel.2016.11.015.

4. Dawidczyk, C. M.; Kim, C.; Park, J. H.; Russell, L. M.; Lee, K. H.; Pomper, M. G.; Searson, P. C. State-of-the-art in design rules for drug delivery platforms: lessons learned from FDA-approved nanomedicines. *J. Control. Release* **2014,** *187*, 133-144. DOI: 10.1016/j.jconrel.2014.05.036.

5. Liu, Q.; Das, M.; Liu, Y.; Huang, L. Targeted drug delivery to melanoma. *Adv. Drug Deliv. Rev.* **2018,** *127*, 208-221. DOI: 10.1016/j.addr.2017.09.016.

6. Weyers, W. The epidemic' of melanoma between under- and overdiagnosis. *J. Cutan. Pathol.* **2012,** *39* (1), 9-16. DOI: 10.1111/j.1600-0560.2011.01831.x.

7. Leiter, U.; Meier, F.; Schittek, B.; Garbe, C. The natural course of cutaneous melanoma. *J. Surg. Oncol.* **2004,** *86* (4), 172-178. DOI: 10.1002/jso.20079.

8. Li, J.; Wang, Y.; Liang, R.; An, X.; Wang, K.; Shen, G.; Tu, Y.; Zhu, J.; Tao, J. Recent advances in targeted nanoparticles drug delivery to melanoma. *Nanomedicine* **2015,** *11* (3), 769-794. DOI: 10.1016/j.nano.2014.11.006.

9. Insua-Rodriguez, J.; Oskarsson, T. The extracellular matrix in breast cancer. *Adv. Drug Deliv. Rev.* **2016,** *97*, 41-55. DOI: 10.1016/j.addr.2015.12.017.

10. Kouloulias, V. E.; Dardoufas, C. E.; Kouvaris, J. R.; Gennatas, C. S.; Polyzos, A. K.; Gogas, H. J.; Sandilos, P. H.; Uzunoglu, N. K.; Malas, E. G.; Vlahos, L. J. Liposomal doxorubicin in conjunction with reirradiation and local hyperthermia treatment in recurrent breast cancer: a phase I/II trial. *Clin. Cancer Res.* **2002,** *8* (2), 374-382.

11. Jin, S.; Mishra-Kalyani, P. S.; Sridhara, R. Unresectable and Metastatic Melanoma of the Skin. *Ther. Innov. Regul. Sci.* **2018**, in press. DOI: 10.1177/2168479018769286.

12. Kejik, Z.; Jakubek, M.; Kaplanek, R.; Kralova, J.; Mikula, I.; Martasek, P.; Kral, V. Epigenetic agents in combined anticancer therapy. *Future Med. Chem.* **2018,** *10* (9), 1113-1130. DOI: 10.4155/fmc-2017-0203.

13. Celli, J. P.; Spring, B. Q.; Rizvi, I.; Evans, C. L.; Samkoe, K. S.; Verma, S.; Pogue, B. W.; Hasan, T. Imaging and photodynamic therapy: mechanisms, monitoring, and optimization. *Chem. Rev.* **2010,** *110* (5), 2795-2838. DOI: 10.1021/cr900300p.

14. Hong, E. J.; Choi, D. G.; Shim, M. S. Targeted and effective photodynamic therapy for cancer using functionalized nanomaterials. *Acta Pharm. Sin. B* **2016,** *6* (4), 297-307. DOI: 10.1016/j.apsb.2016.01.007.

15. Chen, Q.; Wen, J.; Li, H.; Xu, Y.; Liu, F.; Sun, S. Recent advances in different modal imaging-guided photothermal therapy. *Biomaterials* **2016,** *106*, 144-166. DOI: 10.1016/j.biomaterials.2016.08.022.

16. Yano, S.; Hirohara, S.; Obata, M.; Hagiya, Y.; Ogura, S.; Ikeda, A.; Kataoka, H.; Tanaka, M.; Joh, T. Current states and future views in photodynamic therapy. *J. Photochem. Photobiol. C Photochem. Rev.* **2011,** *12* (1), 46-67. DOI: 10.1016/j.jphotochemrev.2011.06.001.

17. Chatterjee, D. K.; Fong, L. S.; Zhang, Y. Nanoparticles in photodynamic therapy: an emerging paradigm. *Adv. Drug Deliv. Rev.* **2008,** *60* (15), 1627-1637. DOI: 10.1016/j.addr.2008.08.003.

18. Castano, A. P.; Demidova, T. N.; Hamblin, M. R. Mechanisms in photodynamic therapy: part one-photosensitizers, photochemistry and cellular localization. *Photodiagnosis Photodyn. Ther.* **2004,** *1* (4), 279-293. DOI: 10.1016/S1572-1000(05)00007-4.

19. Guo, M.; Mao, H. J.; Li, Y. L.; Zhu, A. J.; He, H.; Yang, H.; Wang, Y. Y.; Tian,

X.; Ge, C. C.; Peng, Q. L.; Wang, X. Y.; Yang, X. L.; Chen, X. Y.; Liu, G.; Chen, H. B. Dual imaging-guided photothermal/photodynamic therapy using micelles. *Biomaterials* **2014,** *35* (16), 4656-4666. DOI: 10.1016/j.biomaterials.2014.02.018.

20. Overgaard, J. The current and potential role of hyperthermia in radiotherapy. *Int. J. Radiat. Oncol. Biol. Phys.* **1989,** *16* (3), 535-549. DOI: 10.1016/0360-3016(89)90470-7.

21. Moon, H. K.; Lee, S. H.; Choi, H. C. In vivo near-infrared mediated tumor destruction by photothermal effect of carbon nanotubes. *ACS Nano* **2009,** *3* (11), 3707-3713. DOI: 10.1021/nn900904h.

22. Zheng, M.; Yue, C.; Ma, Y.; Gong, P.; Zhao, P.; Zheng, C.; Sheng, Z.; Zhang, P.; Wang, Z.; Cai, L. Single-step assembly of DOX/ICG loaded lipid--polymer nanoparticles for highly effective chemo-photothermal combination therapy. *ACS Nano* **2013,** *7* (3), 2056-2067. DOI: 10.1021/nn400334y.

23. Wilhelm, S.; Tavares, A. J.; Dai, Q.; Ohta, S.; Audet, J.; Dvorak, H. F.; Chan, W. C. W. Analysis of nanoparticle delivery to tumours. *Nat. Rev. Mat.* **2016,** *1* (5), 16014. DOI: 10.1038/natrevmats.2016.14.

24. Goldberg, E. P.; Hadba, A. R.; Almond, B. A.; Marotta, J. S. Intratumoral cancer chemotherapy and immunotherapy: opportunities for nonsystemic preoperative drug delivery. *J. Pharm. Pharmacol.* **2002,** *54* (2), 159-180. DOI: 10.1211/0022357021778268.

25. Kim, D. Y.; Kwon, D. Y.; Kwon, J. S.; Park, J. H.; Park, S. H.; Oh, H. J.; Kim, J. H.; Min, B. H.; Park, K.; Kim, M. S. Synergistic anti-tumor activity through

combinational intratumoral injection of an in-situ injectable drug depot. *Biomaterials* **2016,** *85*, 232-245. DOI: 10.1016/j.biomaterials.2016.02.001.

26. Bakalova, R.; Zhelev, Z.; Aoki, I.; Masamoto, K.; Mileva, M.; Obata, T.; Higuchi, M.; Gadjeva, V.; Kanno, I. Multimodal silica-shelled quantum dots: direct intracellular delivery, photosensitization, toxic, and microcirculation effects. *Bioconjug. Chem.* **2008,** *19* (6), 1135-1142. DOI: 10.1021/bc700431c.

27. Xia, B.; Wang, B.; Shi, J. S.; Zhang, Y.; Zhang, Q.; Chen, Z. Y.; Li, J. C. Photothermal and biodegradable polyaniline/porous silicon hybrid nanocomposites as drug carriers for combined chemo-photothermal therapy of cancer. *Acta Biomater.* **2017,** *51*, 197-208. DOI: 10.1016/j.actbio.2017.01.015.

28. Wang, X. J.; Li, H. C.; Liu, X. P.; Tian, Y.; Guo, H. S.; Jiang, T.; Luo, Z. M.; Jin, K.; Kuai, X. P.; Liu, Y.; Pang, Z. Q.; Yang, W. L.; Shen, S. Enhanced photothermal therapy of biomimetic polypyrrole nanoparticles through improving blood flow perfusion. *Biomaterials* **2017,** *143*, 130-141. DOI: 10.1016/j.biomaterials.2017.08.004.

29. Treger, J. S.; Priest, M. F.; Iezzi, R.; Bezanilla, F. Real-time imaging of electrical signals with an infrared FDA-approved dye. *Biophys. J.* **2014,** *107* (6), L09-12. DOI: 10.1016/j.bpj.2014.07.054.

30. Yaseen, M. A.; Yu, J.; Jung, B.; Wong, M. S.; Anvari, B. Biodistribution of encapsulated indocyanine green in healthy mice. *Mol. Pharm.* **2009,** *6* (5), 1321-1332. DOI: 10.1021/mp800270t.

31. Zhang, X. H.; Li, Q.; Sun, X. D.; Zhang, B. L.; Kang, H. X.; Zhang, F. L.; Jin, Y.

G. Doxorubicin-Loaded Photosensitizer-Core pH-Responsive Copolymer Nanocarriers for Combining Photodynamic Therapy and Chemotherapy. *ACS Biomat. Sci. Engineer.* **2017,** *3* (6), 1008-1016. DOI: 10.1021/acsbiomaterials.6b00762.

32. Zhang, Z.; Achilefu, S. Synthesis and evaluation of polyhydroxylated near-infrared carbocyanine molecular probes. *Org. Lett.* **2004,** *6* (12), 2067-2070. DOI: 10.1021/ol049258a.

33. Wu, Y.; Cheng, C.; Jiao, L.; Yu, C.; Wang, S.; Wei, Y.; Mu, X.; Hao, E. beta-Thiophene-fused BF2-azadipyrromethenes as near-infrared dyes. *Org. Lett.* **2014,** *16* (3), 748-751. DOI: 10.1021/ol4034622.

34. Zhang, X. F.; Lin, Y.; Guo, W. F.; Zhu, J. Z. Spectroscopic insights on imidazole substituted phthalocyanine photosensitizers: Fluorescence properties, triplet state and singlet oxygen generation. *Spectrochim. Acta A Mol. Biomol. Spectr.* **2014,** *133*, 752-758. DOI: 10.1016/j.saa.2014.06.063.

35. Jin, Y.; Tong, L.; Ai, P.; Li, M.; Hou, X. Self-assembled drug delivery systems. 1. Properties and in vitro/in vivo behavior of acyclovir self-assembled nanoparticles (SAN). *Int. J. Pharm.* **2006,** *309* (1-2), 199-207. DOI: 10.1016/j.ijpharm.2005.11.025.

36. Rodrigues, H. F.; Capistrano, G.; Mello, F. M.; Zufelato, N.; Silveira-Lacerda, E.; Bakuzis, A. F. Precise determination of the heat delivery during in vivo magnetic nanoparticle hyperthermia with infrared thermography. *Phys. Med. Biol.* **2017,** *62* (10), 4062-4082. DOI: 10.1088/1361-6560/aa6793.

37. Sun, X.; Qiu, H.; Jin, Y. Highly efficient treatment of aerobic vaginitis with simple acidic buffered gels: The importance of pH and buffers on the

microenvironment of vaginas. *Int. J. Pharm.* **2017,** *525* (1), 175-182. DOI: 10.1016/j.ijpharm.2017.04.026.

38. Zhu, L.; Li, M.; Liu, X.; Du, L.; Jin, Y. Inhalable oridonin-loaded poly(lactic-co-glycolic)acid large porous microparticles for in situ treatment of primary non-small cell lung cancer. *Acta Pharm. Sin. B* **2017,** *7* (1), 80-90. DOI: 10.1016/j.apsb.2016.09.006.

39. Zhu, L.; Li, M.; Liu, X.; Jin, Y. Drug-Loaded PLGA Electrospraying Porous Microspheres for the Local Therapy of Primary Lung Cancer via Pulmonary Delivery. *ACS Omega* **2017,** *2* (5), 2273-2279. DOI: 10.1021/acsomega.7b00456.

40. Hong, E. J.; Choi, D. G.; Shim, M. S. Targeted and effective photodynamic therapy for cancer using functionalized nanomaterials. *Acta Pharm. Sin. B* **2016,** *6* (4), 297-307. DOI: 10.1016/j.apsb.2016.01.007.

41. Oniszczuk, A.; Wojtunik-Kuleszaa, K. A.; Oniszczuk, T.; Kasprzak, K. The potential of photodynamic therapy (PDT)-Experimental investigations and clinical use. *Biomed. Pharmacother.* **2016,** *83*, 912-929. DOI: 10.1016/j.biopha.2016.07.058.

42. Wei, Z.; Gu, Z. Y.; Arvapally, R. K.; Chen, Y. P.; McDougald, R. N., Jr.; Ivy, J. F.; Yakovenko, A. A.; Feng, D.; Omary, M. A.; Zhou, H. C. Rigidifying fluorescent linkers by metal-organic framework formation for fluorescence blue shift and quantum yield enhancement. *J. Am. Chem. Soc.* **2014,** *136* (23), 8269-8276. DOI: 10.1021/ja5006866.

43. Jang, B.; Park, J.-Y.; Tung, C.-H.; Choi, Y. Gold nanorod-photosensitizer complex for near-infrared fluorescence imaging and photodynamic/photothermal

therapy in vivo. *ACS Nano* **2011,** *5*, 1086-1094. DOI: 10.1021/nn102722z

44. Jin, Y.; Zhang, X.; Zhang, B.; Kang, H.; Du, L.; Li, M. Nanostructures of an amphiphilic zinc phthalocyanine polymer conjugate for photodynamic therapy of psoriasis. *Colloids Surf. B Biointerfaces* **2015,** *128*, 405-409. DOI: 10.1016/j.colsurfb.2015.02.038

45. Li, Q.; Jin, Y. G.; Li, M.; Dong, J. X. Drug-Loaded Star-Shaped pH-Responsive Monomolecular Copolymer Nanocarriers for Tumor Targeting and Cancer Therapy. *ACS Biomat. Sci. Engineer.* **2015,** *1* (3), 175-182. DOI: 10.1021/ab5001194.

46. Li, Q.; Yao, W.; Yu, X.; Zhang, B.; Dong, J.; Jin, Y. Drug-loaded pH-responsive polymeric micelles: Simulations and experiments of micelle formation, drug loading and drug release. *Colloids Surf. B Biointerfaces* **2017,** *158*, 709-716. DOI: 10.1016/j.colsurfb.2017.07.063.

47. Kanamala, M.; Wilson, W. R.; Yang, M.; Palmer, B. D.; Wu, Z. Mechanisms and biomaterials in pH-responsive tumour targeted drug delivery: A review. *Biomaterials* **2016,** *85*, 152-167. DOI: 10.1016/j.biomaterials.2016.01.061.

48. Creusat, G.; Rinaldi, A. S.; Weiss, E.; Elbaghdadi, R.; Remy, J. S.; Mulherkar, R.; Zuber, G. Proton sponge trick for pH-sensitive disassembly of polyethylenimine-based siRNA delivery systems. *Bioconjug. Chem.* **2010,** *21* (5), 994-1002. DOI: 10.1021/bc100010k.

49. Stubbs, M.; McSheehy, P. M.; Griffiths, J. R.; Bashford, C. L. Causes and consequences of tumour acidity and implications for treatment. *Mol. Med. Today* **2000,** *6* (1), 15-19. DOI: 10.1016/S1357-4310(99)01615-9.

50. Emi, T. T.; Barnes, T.; Orton, E.; Reisch, A.; Tolouei, A. E.; Madani, S. Z. M.; Kennedy, S. M. Pulsatile Chemotherapeutic Delivery Profiles Using Magnetically Responsive Hydrogels. *ACS Biomat. Sci. Engineer.* **2018,** *4* (7), 2412-2423. DOI: 10.1021/acsbiomaterials.8b00348.

51. Shaul, P.; Steinbuch, K. B.; Blacher, E.; Stein, R.; Fridman, M. Exploring the Effects of Glycosylation and Etherification of the Side Chains of the Anticancer Drug Mitoxantrone. *ChemMedChem* **2015,** *10* (9), 1528-1538. DOI: 10.1002/cmdc.201500274.

52. Yu, X.; Du, L.; Li, Y.; Fu, G.; Jin, Y. Improved anti-melanoma effect of a transdermal mitoxantrone ethosome gel. *Biomed. Pharmacother.* **2015,** *73*, 6-11. DOI: 10.1016/j.biopha.2015.05.002.

53. Yu, X.; Du, L.; Zhu, L.; Liu, X.; Zhang, B.; Fu, G.; Jin, Y. Melanoma therapy with transdermal mitoxantrone cubic phases. *Drug Del.* **2016,** *23* (5), 1565-1570. DOI: 10.3109/10717544.2015.1024898.

54. Dabrowski, J. M.; Arnaut, L. G. Photodynamic therapy (PDT) of cancer: from local to systemic treatment. *Photochem. Photobiol. Sci.* **2015,** *14* (10), 1765-1780. DOI: 10.1039/c5pp00132c.

55. Chen, G.; Wang, Y.; Xie, R.; Gong, S. Tumor-targeted pH/redox dual-sensitive unimolecular nanoparticles for efficient siRNA delivery. *J. Control. Release* **2017,** *259*, 105-114. DOI: 10.1016/j.jconrel.2017.01.042.

56. Vitkin, I. A.; Woolsey, J.; Wilson, B. C.; Anderson, R. R. Optical and thermal characterization of natural (Sepia officinalis) melanin. *Photochem. Photobiol.* **1994,**

59 (4), 455-462. DOI: 10.1111/j.1751-1097.1994.tb05064.x.

57. Godoy, S. E.; Hayat, M. M.; Ramirez, D. A.; Myers, S. A.; Padilla, R. S.; Krishna, S. Detection theory for accurate and non-invasive skin cancer diagnosis using dynamic thermal imaging. *Biomed. Opt. Exp.* **2017,** *8* (4), 2301-2323. DOI: 10.1364/Boe.8.002301.

58. Bonmarin, M.; Le Gal, F. A. Lock-in thermal imaging for the early-stage detection of cutaneous melanoma: a feasibility study. *Comput. Biol. Med.* **2014,** *47*, 36-43. DOI: 10.1016/j.compbiomed.2014.01.008.

59. Mundra, V.; Peng, Y.; Rana, S.; Natarajan, A.; Mahato, R. I. Micellar formulation of indocyanine green for phototherapy of melanoma. *J. Control. Release* **2015,** *220* (Pt A), 130-140. DOI: 10.1016/j.jconrel.2015.10.029.

60. Abo-Elfadl, M. T.; Gamal-Eldeen, A. M.; Elshafey, M. M.; Abdalla, G. M.; Ali, S. S.; Ali, M. R.; Zawrah, M. F. Photothermal therapeutic effect of PEGylated gold nano-semicubes in chemically-induced skin cancer in mice. *J. Photochem. Photobiol. B* **2016,** *164*, 21-29. DOI: 10.1016/j.jphotobiol.2016.09.012.

61. Wang, X.; Zhang, J.; Wang, Y.; Wang, C.; Xiao, J.; Zhang, Q.; Cheng, Y. Multi-responsive photothermal-chemotherapy with drug-loaded melanin-like nanoparticles for synergetic tumor ablation. *Biomaterials* **2016,** *81*, 114-124. DOI: 10.1016/j.biomaterials.2015.11.037.

62. Beebe, S. J.; Lassiter, B. P.; Guo, S. Nanopulse Stimulation (NPS) Induces Tumor Ablation and Immunity in Orthotopic 4T1 Mouse Breast Cancer: A Review. *Cancers (Basel)* **2018,** *10* (4), 97. DOI: 10.3390/cancers10040097.

63. Song, N.; Guo, H.; Ren, J.; Hao, S.; Wang, X. Synergistic anti-tumor effects of dasatinib and dendritic cell vaccine on metastatic breast cancer in a mouse model. *Oncol. Lett.* **2018,** *15* (5), 6831-6838. DOI: 10.3892/ol.2018.8188.

64. F.Sanmamed, M.; Fernández-Landázuri, S.; Rodríguez, C.; D.Lozano, M.; I.Echeveste, J.; Gracia, J. L. P.; Alegre, E.; Carranza, O.; Zubiri, L.; Martín-Algarra, S.; González, A. Relevance of MIA and S100 serum tumor markers to monitor BRAF inhibitor therapy in metastatic melanoma patients. *Clin. Chim. Acta* **2014,** *429*, 168-174. DOI: 10.1016/j.cca.2013.11.034

65. Papetti, M.; Herman, I. M. Mechanisms of normal and tumor-derived angiogenesis. *Am. J. Physiol. Cell Physiol.* **2002,** *282* (5), C947-970. DOI: 10.1152/ajpcell.00389.2001.

66. Li, Y.; Ahmed, F.; Ali, S.; Philip, P. A.; Kucuk, O.; Sarkar, F. H. Inactivation of nuclear factor kappaB by soy isoflavone genistein contributes to increased apoptosis induced by chemotherapeutic agents in human cancer cells. *Cancer Res.* **2005,** *65* (15), 6934-6942. DOI: 10.1158/0008-5472.CAN-04-4604.

67. Oleinick, N. L.; Morris, R. L.; Belichenko, T. The role of apoptosis in response to photodynamic therapy: what, where, why, and how. *Photochem. Photobiol. Sci.* **2002,** *1* (1), 1-21. DOI: 10.1039/b108586g.

68. Zhou, Z. J.; Yan, Y.; Hu, K. W.; Zou, Y.; Li, Y. W.; Ma, R.; Zhang, Q.; Cheng, Y. Y. Autophagy inhibition enabled efficient photothermal therapy at a mild temperature. *Biomaterials* **2017,** *141*, 116-124. DOI: 10.1016/j.biomaterials.2017.06.030.

69. Guissi, N. E.; Li, H.; Xu, Y.; Semcheddine, F.; Chen, M.; Su, Z.; Ping, Q. Mitoxantrone- and Folate-TPGS2k Conjugate Hybrid Micellar Aggregates To Circumvent Toxicity and Enhance Efficiency for Breast Cancer Therapy. *Mol. Pharm.* **2017,** *14* (4), 1082-1094. DOI: 10.1021/acs.molpharmaceut.6b01009.

For Table of Contents Use Only

Intratumorally Injected Photothermal Agent-Loaded Photodynamic Nanocarriers for Ablation of Orthotopic Melanoma and Breast Cancer

Xiaodong Sun, Bo Zhuang, Mengmeng Zhang, Heliu Jiang and Yiguang Jin*